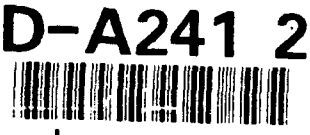

(2)

CONTRACTOR REPORT BRL-CR-674

BRL

FINITE ELEMENT MODEL FOR GAP CONTACT PROBLEMS

ADAM R. ZAK
ZAK TECHNOLOGIES, INC.

AUGUST 1991

U.S. ARMY LABORATORY COMMAND

BALLISTIC RESEARCH LABORATORY
ABERDEEN PROVING GROUND, MARYLAND

NOTICES

Destroy this report when it is no longer needed. DO NOT return it to the originator.

Additional copies of this report may be obtained from the National Technical Information Service, U.S. Department of Commerce, 5285 Port Royal Road, Springfield, VA 22161.

The findings of this report are not to be construed as an official Department of the Army position, unless so designated by other authorized documents.

The use of trade names or manufacturers' names in this report does not constitute indorsement of any commercial product.

UNCLASSIFIED

REPORT DOCUMENTATION PAGE

Form Approved
OMB No. 0704-0188

1. AGENCY USE ONLY (Leave blank)	2. REPORT DATE	3. REPORT TYPE AND DATES COVERED
	August 1991	Final, Oct 83 – Aug 84

4. TITLE AND SUBTITLE

Finite Element Model for Gap Contact Problems

5. FUNDING NUMBERS

PR: 1L162618AH80

6. AUTHOR(S)

Adam R. Zak

7. PERFORMING ORGANIZATION NAME(S) AND ADDRESS(ES)

Zak Technologies Inc.
2310 Belmore Drive
Champaign, IL 61820

8. PERFORMING ORGANIZATION REPORT NUMBER

9. SPONSORING/MONITORING AGENCY NAME(S) AND ADDRESS(ES)

U.S. Army Ballistic Research Laboratory
ATTN: SLCBR-DD-T
Aberdeen Proving Ground, MD 21005-5066

10. SPONSORING/MONITORING AGENCY REPORT NUMBER

BRL-CR-674

11. SUPPLEMENTARY NOTES

12a. DISTRIBUTION/AVAILABILITY STATEMENT

Approved for public release; distribution is unlimited.

12b. DISTRIBUTION CODE

13. ABSTRACT (Maximum 200 words)

A finite element model is developed for structural analysis of axisymmetric geometries with surface contact. The contact occurs when small gaps exist between adjacent parts of the structure and these gaps are closed during the loading cycle. In the model, this phenomenon is simulated by special gap finite elements. Originally, the gap elements have relatively low stiffness, and as surface contact is obtained, the stiffness matrix of these elements is modified to simulate very stiff response in the direction of the contact. The finite element model allows for elastic-plastic and elastic-viscoplastic materials with isotropic or orthotropic properties. The axisymmetric configuration allows for three displacement components in the cylindrical coordinates.

14. SUBJECT TERMS

finite element; model; axisymmetric; gaps; stiffness; displacement; load; contact

15. NUMBER OF PAGES

61

16. PRICE CODE

17. SECURITY CLASSIFICATION OF REPORT	18. SECURITY CLASSIFICATION OF THIS PAGE	19. SECURITY CLASSIFICATION OF ABSTRACT	20. LIMITATION OF ABSTRACT
UNCLASSIFIED	UNCLASSIFIED	UNCLASSIFIED	UL

UNCLASSIFIED

INTENTIONALLY LEFT BLANK.

TABLE OF CONTENTS

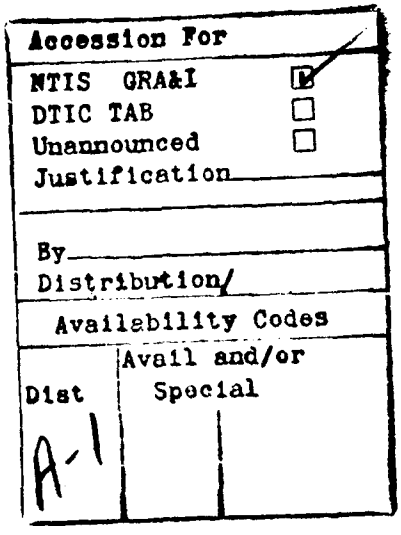

LIST OF FIGURES

1. INTRODUCTION

The objective of the present investigation is to develop a finite element model for use in contact problems. These problems occur when small clearance exists between adjacent parts of the structure and this clearance is closed during the load cycle. This leads to contact between materials which modified the structural response. The structural contact problem is essentially a nonlinear phenomenon as illustrated by the well-known Hertz contact problem (Gaertner 1977). The nonlinear nature of the contact problem makes it suitable for solution by the finite element solution. The finite element method has two distinct approaches for solving contact problems, which include the direct method and the gap element method.

In the direct method, a number of approaches can be used. One such approach involves formulating the problem with constraints. The solution is then performed with a suitable mathematical programming technique. The direct method solves contact problems through some sort of special mathematical programming technique. Hung and Saxce (1980) describe a method which uses variational principles to solve contact problems. Specifically, the contact problem is equivalent to a minimization of potential energy with constraints on the displacements so that surface overlap does not take place. One disadvantage of this approach is that it is difficult to append to existing finite element codes.

Another direct approach is to have the finite element program check for contact, and when it is established, the finite element grid is then modified. The disadvantage of this approach is that when the contact occurs, the finite element grid changes and, consequently, the total number of degrees of freedom is also changed. For relatively small problems, this approach does not lead to too much difficulty, but has definite disadvantages as the complexity of the structure increases.

The second approach is to use gap finite elements to simulate the contact characteristics. These elements have to have low stiffness for open gap and very large stiffness as contact occurs. A number of variations of this approach have been tried (Mahmoud, Salomon, and Marks 1982; Stadter and Weiss 1979). One advantage of the gap element approach is that the finite element grid does not change as the contact occurs. The second advantage is that this approach can easily be appended to existing finite element programs.

The objective in the present investigation is to incorporate the gap element model into an axisymmetric finite element analysis. The analysis into which the contact capability is to be incorporated is the program SAGA (Zak 1974, 1975). SAGA program is an elastic code with three degrees of freedom in the displacements. Consequently, SAGA permits not only the regular axisymmetric solutions, but also torsional solutions. The program allows for quite general loading conditions including concentrated, distributed, inertia, and thermal loads. Material properties are fully orthotropic, allowing for axis of orthotropy to vary in the meridian plane as well as in helical direction.

A further objective is to have the gap element capability in an elastic-plastic program. Consequently, the first step in the investigation is to convert SAGA into elastic-plastic code. The model for an elastic-plastic model has been developed previously for finite elements in connection with previous studies (Zak, Craddock, and Drysdale 1979; Hill 1948). The conversion of SAGA into elastic-plastic versions involves two steps. The first step is to change the program into incremental loading. The second step is to introduce the yield condition and the calculation of incremental plastic stress-strain relations (Zak, Craddock, and Drysdale 1979). In addition to this capability, it is also intended to have one version of the model capable of elastic-viscoplastic analysis. This modification is a relatively straightforward extension of the elastic-plastic model.

The introduction of the gap element capability into the modified version of SAGA will involve a number of steps. The first of these involves certain geometric parameters which describe the gap position in the element system as well as the size and orientation of the gap. The position and orientation of the gap will determine which points can contact as the gap closes under load. The second step is to have the computer program possess a systematic way to check for contact. After the contact has been established, the program has to modify the stiffness of the gap elements to simulate closure. As two nodal points contact, they may not move relative to each other perpendicular to the contact surface. However, tangential motion has to be allowed.

The present report discusses the various steps necessary to achieve these objectives.

2. INCREMENTAL ANALYSIS

2.1 Load Increments. The development of the incrementally loaded finite element model is necessary for two reasons. Even if the material properties were to be taken to be linear, it is necessary to increment the analysis for the purpose of the contact solution. The contact problem, even for elastic materials, is a nonlinear phenomenon and, therefore, in order to perform this part of the solution, the load has to be applied by increments. At each increment, the contact conditions have to be checked, and if new contact is established, the gap elements are modified for the next increment of load.

Incremental analysis is also necessary for the purpose of handling nonelastic materials for which incremental stress-strain relations have to be used. These relations are load dependent, as will be shown in the next section.

2.2 Incremental Elastic-Plastic Stress-Strain. The present elastic-plastic material will be based on Hill's criterion (Hill 1948) for orthotropic materials. In addition, it is desired to include in the material model the effects of kinematic hardening. This hardening phenomenon has been proposed for isotropic materials (Calladine 1969) and extended to orthotropic materials (Zak, Craddock, and Drysdale 1979).

To describe the plastic work hardening behavior of a material, three things are needed:

(1) an initial yield condition

(2) a flow rule relating plastic strain increments to the stress and the stress increment

(3) a hardening rule.

For this work, the Hill's yield criterion (Hill 1948) for orthotropic materials was chosen. This reduces to the von Mises-Hencky yield condition if the material is isotropic. The Hill's condition will be discussed more fully later, but it can be represented symbolically as follows:

$$F(\sigma_{ij}) = 1 \tag{1}$$

at the point where yielding occurs.

The Prager or the kinematic strain hardening rule was used (Calladine 1969). This hardening rule assumes that the yield surface retains its initial size and shape but undergoes a translation in the direction of the plastic strain increment. After plastic flow begins, the yield surface can be written as the following:

$$F(\sigma_{ij} - \alpha_{ij}) = 1 , \tag{2}$$

where the α_{ij} represents the translation of yield surface. The assumption that this translation is in the direction of the plastic strain increment can be written as the following:

$$d\alpha_{ij} = c\, d\varepsilon^{p}_{ij} , \tag{3}$$

where c is a constant for the material.

The flow rule chosen was also due to von Mises; namely,

$$d\varepsilon^{p}_{ij} = \frac{\partial F}{\partial \sigma_{ij}} d\lambda \; ; \; d\lambda \geq 0 . \tag{4}$$

The scalar $d\lambda$ in Equation 4 can be determined by the fact that the stresses remain on the yield surface during plastic flow. This condition can be expressed as the following:

$$(d\sigma_{ij} - d\alpha_{ij}) \frac{\partial F}{\partial \sigma_{ij}} = 0 . \tag{5}$$

Substituting from Equations 3 and 4 into Equation 5 gives the following:

$$\left(d\sigma_{ij} - c \frac{\partial F}{\partial \sigma_{ij}} d\lambda \right) \frac{\partial F}{\partial \sigma_{ij}} = 0 . \tag{6}$$

Solving Equation 6 for $d\lambda$ gives the following:

$$d\lambda = \left\{ \frac{1}{c} \frac{\partial F}{\partial \sigma_{ij}} d\sigma_{ij} \right\} \left\{ \frac{\partial F}{\partial \sigma_{kl}} \frac{\partial F}{\partial \sigma_{kl}} \right\}^{-1} . \tag{7}$$

The total strain increment is the sum of the elastic and the plastic strain increments. Thus,

$$d\varepsilon_{ij}^{e} = d\varepsilon_{ij} - d\varepsilon_{ij}^{p} , \tag{8}$$

where $d\varepsilon_{ij}$ is the total strain increment.

Substituting for $d\varepsilon_{ij}^{e}$ in the elastic stress-strain relationship gives the following:

$$d\sigma_{ij} = E_{ijkl} \left[d\varepsilon_{kl} - d\varepsilon_{kl}^{p} \right] , \tag{9}$$

where E_{ijkl} is the elastic stress-strain matrix.

Equation 5 can be rewritten as the following:

$$\left(d\sigma_{ij} - c\, d\varepsilon_{ij}^{p} \right) \frac{\partial F}{\partial \sigma_{ij}} = 0 . \tag{10}$$

Then, substituting Equations 4, 7, and 9 into Equation 10 gives the following:

$$\left\{ E_{ijkl} \left[d\varepsilon_{kl} - \frac{\partial F}{\partial \sigma_{kl}} d\lambda \right] - c \frac{\partial F}{\partial \sigma_{ij}} d\lambda \right\} \frac{\partial F}{\partial \sigma_{ij}} = 0 . \tag{11}$$

This can be rewritten as the following:

$$E_{ijkl}\, d\varepsilon_{kl}\, \frac{\partial F}{\partial \sigma_{ij}} = \left\{ E_{ijkl}\, \frac{\partial F}{\partial \sigma_{ij}}\, \frac{\partial F}{\partial \sigma_{kl}} + c\, \frac{\partial F}{\partial \sigma_{ij}}\, \frac{\partial F}{\partial \sigma_{ij}} \right\} d\lambda \,. \tag{12}$$

Then, defining the bracketed term as *1/D* where *D* is the scalar,

$$D = \left\{ E_{ijkl}\, \frac{\partial F}{\partial \sigma_{kl}}\, \frac{\partial F}{\partial \sigma_{ij}} + c\, \frac{\partial F}{\partial \sigma_{ij}} + \frac{\partial F}{\partial \sigma_{ij}} \right\}^{-1} \,. \tag{13}$$

Equation 12 can be written as the following:

$$d\lambda = D\, E_{ijkl}\, \frac{\partial F}{\partial \sigma_{ij}}\, d\varepsilon_{kl} \,. \tag{14}$$

Substituting Equation 14 into Equation 4 gives a relation between the total strain increment and the plastic strain increment as follows:

$$d\varepsilon_{ij}^{p} = D\, E_{mnkl}\, \frac{\partial F}{\partial \sigma_{mn}}\, \frac{\partial F}{\partial \sigma_{ij}}\, d\varepsilon_{kl} \,, \tag{15}$$

or

$$d\varepsilon_{ij}^{p} = C_{ijkl}\, d\varepsilon_{kl} \,, \tag{16}$$

where C_{ijkl} is defined from Equation 15.

Then, Equation 9 can be written as the following:

$$d\sigma_{kl} = \left[E_{ijkl} - E_{klmn}\, C_{mnij} \right] d\varepsilon_{ij} \,, \tag{17}$$

or

$$d\sigma_{ij} = A_{ijkl}\, d\varepsilon_{kl} \,, \tag{18}$$

where

$$A_{ijkl} = \left[E_{ijkl} - E_{ijmn} C_{mnkl}\right] . \tag{19}$$

For the isotropic case, c can be evaluated from a uniaxial test. It can be shown that

$$c = \frac{2}{3} \frac{E \cdot E_T}{E - E_T} \,, \tag{20}$$

where E_T is the tangent modulus, and E is Young's Modulus. In general, E_T will depend on the stress state at a given time. Thus, by knowing the elastic constants and the tangent modulus, the stresses can be obtained from the total strains.

2.3 Application to Orthotropic Materials. In the previous section, the incremental stress-strain relations have been developed symbolically in terms of the orthotropic yield function. The specific expression for the Hill's yield criterion is given by the following:

$$F(\sigma_{ij}) = \frac{\sigma_{11}^2}{Y_{11}^2} + \frac{\sigma_{22}^2}{Y_{22}^2} + \frac{\sigma_{33}^2}{Y_{33}^2} + \frac{\sigma_{12}^2}{Y_{12}^2} + \frac{\sigma_{23}^2}{Y_{23}^2} + \frac{\sigma_{13}^2}{Y_{13}^2} + \bar{Y}_{11}\sigma_{22}\sigma_{33}$$

$$+ \bar{Y}_{22}\sigma_{11}\sigma_{33} + \bar{Y}_{33}\sigma_{11}\sigma_{22} = 1 \,, \tag{21}$$

where Y_{11}, Y_{22}, and Y_{33} are the yield stresses in simple tension in the three orthotropic directions, and Y_{12}, Y_{23}, and Y_{13} are the corresponding yield stresses in simple shear. The $\bar{Y}$ terms are functions of the yield stresses. These functions include the following:

$$\bar{Y}_{11} = \frac{1}{Y_{11}^2} - \frac{1}{Y_{22}^2} - \frac{1}{Y_{33}^2} ,$$

$$\bar{Y}_{22} = \frac{1}{y_{22}^2} - \frac{1}{Y_{33}^2} - \frac{1}{Y_{11}^2} ,$$

$$\bar{Y}_{33} = \frac{1}{Y_{33}^2} - \frac{1}{Y_{11}^2} - \frac{1}{Y_{22}^2} . \qquad (22)$$

Equation 21 can be corrected for strain hardening by substituting for stresses as shown in Equations 1 and 2. Using Equation 21 after it has been modified for strain hardening as illustrated by Equation 2, it is possible to differentiate the yield function relative to stress (Zak, Craddock, and Drysdale 1979). These relations then can be used in the previous section to evaluate the incremental stress-strain relations given by Equation 18.

There remains the question of evaluating the hardening parameter, *C*. This was evaluated from a uniaxial test in the isotropic case, but there are three uniaxial tests which can give three different results in the orthotropic case. Consequently, in order to evaluate the hardening parameter for orthotropic materials, some limitations are placed on the orthotropic properties (Zak, Craddock, and Drysdale 1979). One of these is that the material is transversely orthotropic; that is, directions 2 and 3 are identical. It can be shown then (Zak, Craddock, and Drysdale 1979) that the hardening can be related to testing in the orthotropic direction 1:

$$C = \frac{2}{3} \frac{E_{11} \cdot E_{11_T}}{E_{11} - E_{11_T}} . \qquad (23)$$

2.4 Elastic-Plastic SAGA. Once the incremental elastic-plastic relations have been obtained, the next step is to implement these into the SAGA program to create an elastic-plastic version of this program. A flow chart for the new version of SAGA is shown in Figure 1. This version is labeled SAGAEP. The most noticeable difference between this version and the original SAGA is the addition of two new subroutines ELPLSS and YIELD. Subroutine YIELD is used to determine orthotropic yield conditions, and ELPLSS evaluates

incremental stress-strain relations in the plastic region. Less obvious changes involve modification of existing SAGA subroutines, and these include MAIN, QUAD, STIFF, and STRESS.

3. GAP GEOMETRY

3.1 Gap Position. In the formulation of gap elements, there are a number of geometric parameters which either have to be set by input or calculated internally in the program. The first of these parameters has to do with defining the direction of the gap. This direction is in terms of an I-J grid. The I-J coordinate system will locate elements and nodal points. To illustrate how nodal points are located, take a typical element in an I-J grid (Figure 2). This element has nodal point IX(N,1) located at the corner that lies closest to the origin. The remaining three nodal points IX(N,2), IX(N,3), and IX(N,4) are obtained by moving in the counterclockwise direction around the element.

The direction of the gap will depend on an inputted parameter called the principal gap direction. As an example, if the principal gap direction is chosen to be 1, then the gap direction will be parallel to the J-axis, while the direction of closure will be parallel to the I-axis (Figure 3). If the principal gap direction is set to 2, the direction of the gap will be parallel to the I-axis, while the gap closure will be in the J-axis direction (Figure 4).

3.2 Determining Nodal Pairs. The gap direction will determine which node points will be opposite one another along the gap. This information is important for reasons that will be shown in the following sections. Simply stated, these reasons include the following. First, the program must know which node points to pair and then test for contact; and secondly, when contact is established, the nodal point pairs will be used to properly modify gap element material properties. Referring to Figure 3, if the principal gap direction is set to 1, then the two nodal pairs for the element are (IX[N,1], IX[N,2]) and (IX[N,3], IX[N,4]). Similarly, for a principal gap direction of 2, the two pairs are (IX[N,1], IX[N,4]) and (IX[N,2], IX[N,3]), as shown in Figure 4.

3.3 Gap Orientation. Another geometric parameter has to do with the orientation of the gap elements relative to the R-Z axes. This orientation will be used to transform nodal

positions and nodal displacements into a coordinate system where one axis coincides with the direction of the gap, while the other axis coincides with the direction of closure. The second use of the gap orientation will insure that gap material properties will only stiffen in the direction of closure once contact is established.

Once the principal gap direction is determined, the angle of the gap can be calculated. This angle is defined in a manner indicated by Figure 5. As an example, take a typical element with a principal gap direction of 1 and nodal points *I1, I2, I3,* and *I4* [equal to IX(N,1), IX(N,2), IX(N,3), and IX(N,4), respectively]. The angle β will be calculated by first producing a mean line through the element (Figure 6). The coordinates of points 1 and 2 are, respectively, included in the following:

$$\frac{R(I1) + R(I4)}{2} \quad , \quad \frac{Z(I1) + Z(I4)}{2} \tag{24}$$

$$= (Rmean1 \ , \ Zmean1) \ ,$$

$$\frac{R(I2) + R(I3)}{2} \quad , \quad \frac{Z(I2) + Z(I3)}{2} \tag{25}$$

$$= (Rmean2 \ , \ Zmean2) \ .$$

Using Equations 24 and 25, the angle β can be calculated by using the following:

$$\beta = ARCtan \quad \frac{(Rmean2 - Rmean1)}{(Zmean2 - Zmean1)} \ . \tag{26}$$

This definition of β will have coordinate axis N coincident with the direction of closure, and coordinate axis T coincident with the gap direction.

If the principal gap direction is equal to 2, the angle calculation will be the same as previously mentioned, except that Equations 24 and 25 will be replaced by the following:

$$\frac{R(I1) + R(I2)}{2} \quad , \quad \frac{Z(I1) + Z(I2)}{2} \tag{27}$$

$$= (Rmean1 \ , \ Zmean1) \ ,$$

$$\frac{R(I3) + R(I4)}{2} \quad , \quad \frac{Z(I3) + Z(I4)}{2} \tag{28}$$

$$= (Rmean2 \ , \ Zmean2) \ .$$

The last geometric parameter deals with the distance between two nodal points of a given nodal pair. This distance in found by using the following relationship:

$$\text{gap size} = \sqrt{[R(1) - R(2)]^2 + [Z(1) - Z(2)]^2} \ , \tag{29}$$

where *R(1)* and *Z(1)* are the R, Z coordinates of the first node point, and *R(2)*, *Z(2)* are the R, Z coordinates of the second node point.

4. TESTING FOR CONTACT AND LOAD FACTORS

4.1 Testing for Contact. The gap finite elements are designed to simulate the real behavior of gaps. Real gaps will have no resistance to closure before opposing material faces contact. Consequently, the gap elements must possess very low stiffness. After surface contact has been established, the elements must now become very stiff in order for the two surfaces in contact to have no relative motion perpendicular to the surface. The change of the gap element properties will be initiated when the contact between any nodal points is achieved. The check for surface contact is done by comparing the relative motion of nodal pairs described previously. Since the analysis has already been put in an incremental form for the elastic-plastic analysis, it becomes a simple matter to check for contact at each load increment.

Determining whether or not opposing node points have contacted is done by first transforming nodal displacements and nodal positions into a new coordinate system. This coordinate system coincides with the gap direction. The coordinate axis T coincides with the direction of the gap, and coordinate axis N coincides with the direction of closure. The transformation of nodal displacements from the r, z, θ coordinate system to the N, T, S coordinate system is of the following form:

$$\begin{Bmatrix} u_N \\ u_T \\ u_S \end{Bmatrix} = [T] \begin{Bmatrix} u_R \\ u_Z \\ u_\theta \end{Bmatrix}, \tag{30}$$

where u_r, u_z, and u_θ are the nodal displacements in the r, z, and θ directions, respectively, and u_N, u_T, and u_S are the nodal displacements in the N, T, and S directions, respectively.

The transformation matrix $[T]$ is as follows:

$$[T] = \begin{bmatrix} SIN\beta & COS\beta & 0 \\ -COS\beta & SIN\beta & 0 \\ 0 & 0 & 1.0 \end{bmatrix}, \tag{31}$$

where the angle β is defined by Equation 26. As can be seen in Equation 31, the coordinate axes θ and S will always coincide in this transformation.

The transformation of nodal position is similar to the transformation of nodal displacements. This transformation is of the following form:

$$\begin{Bmatrix} P_N \\ P_T \end{Bmatrix} = [T'] \begin{Bmatrix} P_r \\ P_z \end{Bmatrix}, \tag{32}$$

where P_r and P_z are the nodal positions in the r and z directions respectively, and P_N and P_T are the nodal positions in the N and T directions, respectively.

The transformation matrix is as follows:

$$[T'] = \begin{bmatrix} SIN\beta & COS\beta \\ -COS\beta & SIN\beta \end{bmatrix}. \tag{33}$$

The second step in the test for contact involves updating nodal positions in the *N* direction. The updating occurs at the end of every load step; this can be represented by the following:

$$P_N\,(updated) = P_N\,(original) + u_N\,(total)\,, \tag{34}$$

where $P_N\,(updated)$ and $P_N\,(original)$ are the updated and original node positions in the *N* direction, respectively. The term u_N (total) is the total displacement of the node point in the *N* direction at the end of the load step.

The contact condition of an opposing node point pair can be determined by using the updated nodal positions. This is done by comparing the difference of the two original positions to the difference of the two updated positions. This comparison can be represented by the following:

$$\frac{P_N^1\,(original) - P_N^2\,(original)}{P_N^1\,(updated) - P_N^2\,(updated)}\,, \tag{35}$$

where *1* and *2* represent the first and second node points of the node pair, respectively. If Equation 35 is positive, contact between the opposing node points has not taken place. If Equation 35 is negative, however, the opposing node points have overlapped (i.e., crossed over one another).

4.2 Load Factors. When real gaps close, the two opposing material faces will never overlap one another. For an effective simulation of real gaps, this behavior must be duplicated in the program. It is conceivable that a nodal pair that is not contacting at the end of a given load step can be overlapping at the end of the next load step. This can occur because the program only checks for contact at discrete intervals and not continuously. The program handles the problem of overlapping by splitting load steps. The first step in this process takes all the nodal pairs that are overlapping at the end of a given load step and calculates a factor for each one that depends on the degree of overlap.

The calculation of the load factor is best illustrated by the use of an example. Take a nodal pair in which the gap size closes by three units in load step while the amount of

overlap at the end of load step is one unit. The factor for the previous nodal pair will be calculated by the following:

$$1 - \frac{1 = \text{overlap}}{3 = \text{gap closure}} = .666 = \text{load factor} . \qquad (36)$$

Simply stated, if we multiply load step load by .666, we will have a situation where the load is just large enough to make the previous nodal pair contact. It is possible to have a situation where more than one nodal pair is overlapping; in this case, the program will determine the smallest load factor and will multiply the load by that amount.

When the load step is multiplied by the load factor, there remains a part of the load that has yet to be applied. As an example, if a load factor of .6 is calculated for a load step of 1,000 lb, an additional load of 400 lb remains. This calculation can be represented by the following steps:

1,000 lb	-	original load step
x .6	-	load factor
600 lb	-	reduced load step ,

1,000 lb	-	original load step
-600 lb	-	reduced load step
400 lb	-	unrun portion of the load .

The procedure used in the program involves applying the residue force as an additional load step.

5. GAP ELEMENT STIFFNESS

5.1 Stiffness Matrix for Gap Elements. As was stated previously, gap element material properties will change when contact occurs. Before contact, the relative stiffness between the opposing material faces is zero. After contact, the stiffness between the faces is theoretically infinite. For an effective contact analysis, this stiffness behavior must be simulated by the program. With real gaps, the change from a soft material to a stiff material will occur at all areas of contact. Since the finite element program only checks for contact at discrete locations (namely, the location of nodal point pairs), this will be simulated by a stiffness

change between opposing node points. This simulation is good as long as the nodal pairs are not spaced too far apart.

In the present model, gap material properties are changed by modifying gap element stiffness matrices directly. These stiffness matrices are calculated in a nodal system where the degrees of freedom are defined as in Figure 7. The stiffness matrices of the three-dimensional quadrilateral elements in the N, S, T system have the following form: S_{ij} where $i, j = 1,12$. As in all stiffness matrices, the rows of the matrix correspond to the force in question, and the columns correspond to the degrees of freedom. As an example, force 1 will be related to the 12 degrees of freedom by the following:

$$\begin{aligned} F_1 = {} & S_{1,1}u_1 + S_{1,2}u_2 + S_{1,3}u_3 + S_{1,4}u_4 \\ & + S_{1,5}u_5 + S_{1,6}u_6 + S_{1,7}u_7 \\ & + S_{1,8}u_8 + S_{1,9}u_9 + S_{1,10}u_{10} \\ & + S_{1,11}u_{11} + S_{1,12}u_{12} , \end{aligned} \tag{37}$$

where the u terms are the displacements corresponding to the indicated degrees of freedom.

The stiffness between two degrees of freedom can be changed by modifying force equations such as Equation 37. Assume that the relative stiffness between degrees of freedom 1 and 4 needs to be increased. In Equation 37, this is done by setting $S_{1,4}$ equal to the negative of $S_{1,1}$, and increasing the value of $S_{1,1}$. Equation 37 now becomes the following:

$$\begin{aligned} F_1 = {} & S_{1,1}(u_1 - u_4) + S_{1,2}u_2 + S_{1,3}u_3 \\ & + S_{1,5}u_5 + S_{1,6}u_6 + S_{1,7}u_7 + S_{1,8}u_8 \\ & + S_{1,9}u_9 + S_{1,10}u_{10} + S_{1,11}u_{11} + S_{1,12}u_{12} . \end{aligned} \tag{38}$$

In a similar manner, the coefficient $S_{4,1}$ is set equal to the negative of $S_{4,4}$ in the equation for force 4:

$$F_4 = S_{4,4}(u_4 - u_1) + S_{1,2}u_2 + S_{1,3}u_3$$

$$+ S_{1,5}u_5\ S_{1,6}u_6 + S_{1,7}u_7 + S_{1,8}u_8$$

$$+ S_{1,9}u_9 + S_{1,10}u_{10} + S_{1,11}u_{11} + S_{1,12}u_{12}\ . \qquad (39)$$

Since all stiffness matrices are symmetric, the following is true:

$$S_{1,4} = S_{4,1}\ . \qquad (40)$$

Furthermore, using Equation 40,

$$S_{1,1} = S_{4,4}\ . \qquad (41)$$

As can be seen in Equations 38 and 39, the relative stiffness between the two degrees of freedom is governed by the magnitude of $S_{1,1}$ ($=S_{4,4}$). The result of this step is that now the relative motion of points 1 and 4 will be zero in the normal direction N.

5.2 Transformation of Stiffness Matrices. One use of gap element orientation involves the transformation of stiffness matrices. The program assembles the global stiffness matrix in the r, z, and θ direction coordinates. When gaps close, the change in material properties occurs in the direction of closure, which is defined in the N, S, T coordinates. This problem is handled by first modifying the element matrices in the N, T, S coordinate system and then transforming them back into the r, z, θ coordinate system.

The matrix transformation is given by the following:

$$[S'] = [H]^T [S] [H]\ , \qquad (42)$$

where $[S]$ and $[S']$ are the element stiffness matrices in the N, T, S and r, z, θ coordinate systems, respectively. The transformation matrix $[H]$ is as follows:

$$[H] = \begin{bmatrix} [T]^T & & & \\ & [T]^T & & \\ & & [T]^T & \\ & & & [T]^T \end{bmatrix}, \tag{43}$$

where $[T]^T$ is the transpose of the transformation matrix defined in Equation 31.

5.3 Gap Material Properties Before Contact. An important issue in this analysis involves modeling gap behavior before any contact between opposing material faces takes place. In the "real world," gaps have no stiffness between opposing faces before contact. In the program, this behavior is simulated by a very soft gap material; the stiffness of the material is small but not zero. The reasons exist for this nonzero stiffness. There are a number of matrix operations in the program which would fail if all coefficients of the stiffness matrix for an element are zero.

5.4 Modeling Various Contact States. A gap element has four different contact states for each value of the principal gap direction. For an element with a principal gap direction of 1 and opposing nodal pairs (1,2) and (3,4) (shown in Figure 8), the following four contact states exist:

State No. 1 - both node pairs not contacting
State No. 2 - (1,2) contacting; (3,4) not contacting
State No. 3 - (1.2) not contacting; (3,4) contacting
State No. 4 - both nodal pairs contacting.

The gap element stiffness matrix will be modified differently for each of the four states. Assume that the element matrix is modified in the N, T, S coordinate system and that the three degrees of freedom at each node are in the N, T, and S directions, respectively. The proper modification of the element stiffness matrix is as follows:

State No. 1 - all matrix elements remain small.

State No. 2 - set $S_{1,1} = S_{4,4} = -S_{1,4} = -S_{4,1}$
= large number relative to other matrix elements.

State No. 3 - set $S_{7,7} = S_{10,10} = -S_{7,10} = -S_{10,7}$
= large number relative to other matrix elements.

State No. 4 - set $S_{1,1} = S_{4,4} = S_{7,7} = S_{10,10}$
$= -S_{1,4} = -S_{4,1} = -S_{7,10} = -S_{10,7}$
= large number relative to other matrix elements.

If the principal gap direction of the element is equal to 2, the gap element stiffness matrix modification will be similar to that shown previously. The only difference between the two modifications will be that now the two nodal pairs are (1,4) and (2,3), as shown in Figure 9. The four possible states of contact are now the following:

State No. 1 - both nodal pairs not contacting
State No. 2 - (1,4) contacting; (2,3) not contacting
State No. 3 - (1,4) not contacting; (2,3) contacting
State No. 4 - both nodal pairs contacting.

The proper modification of the elements stiffness matrix for the four contact states is now the following:

State No. 1 - all elements in the matrix remain small.

State No. 2 - set $S_{1,1} = S_{10,10} = -S_{1,10} = -S_{10,1}$
= large number relative to other matrix elements.

State No. 3 - set $S_{4,4} = S_{7,7} = -S_{4,7} = -S_{7,4}$
= large number relative to other matrix elements.

State No. 4 - set $S_{1,1} = S_{4,4} = S_{7,7} = S_{10,10}$
$= -S_{1,10} = -S_{10,1} = -S_{4,7} = -S_{7,4}$
= large number relative to other matrix elements.

5.5 Magnitude of Stiffness Change. For the different contact states, we increase the magnitude of various matrix elements. A question remains of how much to increase these matrix elements. In theory, as long as the on-diagonal and off-diagonal terms are equal and opposite, they can approach infinity without affecting any other stiffness besides the relative stiffness between the two degrees of freedom in question. In practice, however, as the numbers approach infinity, the round-off error will cause a significant difference between the on-diagonal and off-diagonal terms. The effect of this error will cause an artificial displacement constraint for the two nodal points in the equation. By executing a number of test cases, it has been found that the change in the magnitude in stiffness should be between order of magnitude of 2 and 4. This order of magnitude applies relative to the material surrounding the gap.

5.6 Transverse Slip. The previous section described the procedure developed for modifying the stiffness coefficients for the gap elements normal to the gap direction. If only these coefficients are modified, then the contact points are relatively free to move relative to each other in the direction parallel to the contact surface. However, in a real situation, one would expect that even this motion would be somewhat restricted due to surface friction effects. Consequently, in the present analysis, a very simple model is proposed to simulate this effect.

The effects of friction will be related to the stiffness in the direction of closure. This relationship is made through the use of a frictional coefficient. As an example, if nodal pair (1,2) in an element is contacting, then the following relationships will model friction:

$$S_{2,2} = S_{5,5} = -S_{5,2} = -S_{2,5} = \text{frict}^* S_{1,1} , \tag{44}$$

$$S_{3,3} = S_{6,6} = -S_{3,6} = -S_{6,3} = \text{frict}^* S_{1,1} , \tag{45}$$

where "frict" is the friction coefficient. Equation 44 relates the stiffness in the direction of closure to the stiffness in the direction of the gap. Similarly, Equation 45 relates the stiffness in the direction of closure to the stiffness in the tangential direction.

6. COMPUTER PROGRAM

6.1 General Description. The flow chart for the program incorporating the gap element capability is shown in Figure 10. This program has been designated as SAAC (Structural Analysis Axisymmetric Contact). It is instructive to compare the chart to that of Figure 1 for the elastic-plastic version of SAGA (SAGAEP). The most obvious differences between SAAC and SAGAEP are additions of new subroutines in Figure 10. These subroutines include GAPANG, RETRANS, and TEST. The various steps necessary to implement the gap element capability will be described in the following sections.

6.2 Geometrical Parameters. As described in the previous sections, the geometry of the gap elements is inputted with few parameters, and these are used by the computer program to establish additional information. Most of the geometrical parameters which are established in the program are done in the Subroutine GAPANG. This subroutine is called from MAIN, as shown in Figure 10.

6.3 Contact Test. Testing for contact and the calculation of load factors occurs in Subroutine TEST. TEST is called in Subroutine SOLV after nodal displacements are calculated.

An assumption was made to the load factor analysis to reduce execution time. The assumption is that the contact condition of nodal pairs is determined by the original load step and not by the reduced load step. As an example of this, if a given number of nodal pairs are overlapping at the end of a load step, the program will then assume that these nodal pairs will remain contacted, even though the load step will be reduced. An advantage of this assumption is that original load steps are only split once. A disadvantage, however, is that the program might predict gap closure at a different load as compared to a real structure with the same configuration. This problem can be minimized by keeping load steps small.

6.4 Stiffness Modification. The modification of stiffness and the friction analysis are both done in Subroutine RETRANS. This change of gap material properties takes place in the N, T, S coordinate system, and afterwards, a transformation back into the r, z, θ system is done.

Subroutine RETRANS is called in Subroutine STIFF after the element stiffness matrices are calculated and before the global matrix is assembled.

The Subroutine RETRANS is the remaining new subroutine to be added to convert SAGAEP to SAAC. In addition to the new subroutines, certain existing subroutines had to be modified. The modified subroutines include MAIN, QUAD, SOLV, and STIFF.

7. ELASTIC-VISCOPLASTIC OPTION

7.1 Viscoplastic Model. An additional objective of the present investigation is to develop an elastic-viscoplastic option for the SAAC program. Since this program has already an elastic-plastic material model, it is a relatively straightforward step to include viscoplasticity. The model for the elastic-viscoplastic material has been developed previously (Zak, Craddock, and Drysdale 1979) in conjunction with one version of the SANX program. A similar approach will be used here.

The elastic-viscoplastic option involves incorporating the rate effect in the stress-strain relations. This rate effect is incorporated in an incremental fashion and can be expressed by the following rate-dependent relation:

$$d\sigma_{ij}^{n+1} = A_{ijkl}^{n} \, d\varepsilon_{kl}^{n+1} + \eta \, d\dot{\varepsilon}_{ij}^{vp\,n+1} , \tag{46}$$

where

$d\sigma_{ij}^{n+1}$ is an incremental change in stress from time t_n to t_{n+1} ;

$d\varepsilon_{kl}^{n+1}$ is the incremental change in total strain;

A_{ijkl}^{n} is the incremental, elastic-plastic material properties matrix;

$d\dot{\varepsilon}_{ij}^{vp\,n+1}$ is the incremental change in the viscoplastic strain rate; and

η is the material viscous coefficient.

By using backward difference relations, it can be shown (Zak, Craddock, and Drysdale 1979) that

$$d\dot{\varepsilon}_{ij}^{vp\,n+1} = \dot{\varepsilon}_{ij}^{vp\,n} - \dot{\varepsilon}_{ij}^{vp\,n-1} . \tag{47}$$

Then, Equation 46 becomes the following:

$$d\sigma_{ij}^{n+1} = A_{ijkl}^{n}\, d\varepsilon_{kl}^{n+1} + \eta \left(\dot{\varepsilon}_{ij}^{vp\,n} - \dot{\varepsilon}_{ij}^{vp\,n-1} \right) . \tag{48}$$

By applying the principle of virtual work to equation 48 and making the usual finite element substitutions, the following is obtained:

$$\{F\} - \{f^v\} = [K]\{\delta\} , \tag{49}$$

where $\{f^v\}$ is the viscous force matrix. The $\{f^v\}$ term can be calculated for each element as the following:

$$\{f^v\} = \eta \int_v [B]^T \left(\{\dot{\varepsilon}^{vp\,n}\} - \{\dot{\varepsilon}^{vp\,n-1}\} \right) dV ; \tag{50}$$

and $[K]$ is the stiffness matrix in the following:

$$[K] = \int_v [B]^T [A] [B]\, dV . \tag{51}$$

Thus, using Equations 50 and 51, the viscous rate effects appear as a modification to the force vector which can be calculated at the start of a load increment. This modification is being used in the development of the elastic-viscoplastic option. In order to convert elastic-plastic SAAC program to the elastic-viscoplastic, changes to the program were made in MAIN and the Subroutines STRESS and TRISTF.

8. NUMERICAL EXAMPLES

8.1 Axisymmetric Perfectly Plastic Problem. The purpose of the first example is to check the elastic-plastic capability of the SAAC program. This is done by executing a simple

example for which an analytical elastic-plastic solution is possible (Shield and Ziegler 1958). This example consists of a uniform, isotropic cylinder subject to internal pressure.

The analytical solution (Shield and Ziegler 1958) is valid for elastic perfectly plastic material. The finite element model, on the other hand, is based on incremental stress-strain relation and cannot handle perfectly plastic response. However, by using very small E_T, the finite element approach can simulate very closely perfect plasticity. Consequently, in this example, the value of E_T was chosen to be .001E. The analytical solution results predict the plastic boundary position and the circumferential strain as a function of internal pressure. Before discussing the comparison of these results with the finite element model, it may be noted that the analytical solution uses Tresca yield criterion.

Figure 11 shows the elastic-plastic boundary vs. pressure curves for both the numerical and analytical solutions. As can be seen, the two solutions coincide fairly well, except for a slight difference due to the different yield criterions. In this problem, the Tresca yield criterion will predict yielding at a lower stress as compared to the Von-Mises yield criterion used in the finite element model. This fact will cause the elastic-plastic boundary obtained from the analytical solution to move outward at a faster rate.

The outer surface circumferential strain vs. pressure curves for both the numerical and analytical solutions are shown in Figure 12. Again, the two solutions coincide closely, except for a small difference due to the different yield criterions. The outer surface strains are higher in the analytical solution because yielding occurs at lower loads as compared to the numerical solution.

8.2 Flat Gap—Coarse Grid Problem. The first gap problem studied is an elastic, 12-element configuration where the inner two elements represent the gap. This configuration is shown in Figure 13. The configuration is loaded under external pressure such that sometime during the loading cycle, node points 10 and 11 will come into contact.

Studying the displacement vs. load curves of nodal points 10 and 11 reveals several behaviors (shown in Figure 14). Before contact, nodal point 11 has a large downward displacement per unit load. This behavior is expected since the downward motion of node

point 11 is not resisted by the gap. Node point 10 has a relatively small upward displacement per unit load before contact. This is also expected since node point 10 has no direct downward load to push on it. The only loads affecting node point 10 are transmitted through elements 4 and 7 by shearing forces.

After contact, the behavior of the displacement vs. load curves changes. Downward motion of point 11 is now resisted by its opposing gap force. Node point 10 is pushed down by its opposing face and, in turn, moves downward more rapidly. As can be seen in Figure 14, the relative motion between node points 10 and 11 is zero after contact. The two node points will move together in a manner that matches the classical Lame's solution for thick tubes. This behavior is not surprising since after contact, the configuration will act like a solid axisymmetric structure.

Another important thing to note is that the two node points contact in the middle of a load increment. This causes the program to calculate a load factor and then split the load step. The first portion of the load increment assumes soft gap material properties, while the second portion assumes stiff gap material properties.

Hoop stress vs. load behavior was also studied for this configuration, as shown in Figure 15. Before contact, elements 6 and 9 will carry a larger amount of hoop stress than elements 4 and 7. This is because the upper elements are loaded directly, while the lower elements only have loads transmitted to them by shearing faces. This behavior is in direct opposition to Lame's solution, wherein the lower elements have the highest hoop stresses.

After contact, the hoop stress vs. load curves will be similar to the curves for a solid structure. As can be seen in Figure 15, the hoop stress vs. load curves after contact have the same slope as their corresponding Lame's solution curves.

8.3 Flat Gap—Fine Grid Problem. A configuration with the same dimensions and loading condition as the previous example was analyzed. The only difference between the two examples is the refinement of the element grid. This new configuration is shown in Figure 16. Using this example, the effect of the grid on the contact analysis can be studied.

The load vs. displacement curves for nodal points 58 and 59 are shown in Figure 17. These two nodal points will contact at higher load than their corresponding nodal points in the coarse grid configuration. This is probably due to the additional elements which cause the finite element analysis to model pressure distribution over the structure more realistically.

The hoop stress vs. load curves is shown in Figure 18. The curves exhibit the same behavior as in the coarse grid structure, except for a small difference due to the refinement of the mesh.

8.4 Angled Gap Problem. This example is included to illustrate the capability of handling gaps which are not necessarily oriented along any particular axis. This example involves an elastic, 12-element configuration where the gap is angled with respect to the Z-axis. The configuration and type of loading are shown in Figure 19. The results are shown in Figure 20, which shows the gap size vs. load curve at the location of the nodal pair (10,11). As can be seen, the closure rate of the gap is linear with pressure until contact is established. After contact, the gap size will remain zero for the remaining portion of the loading cycle. This behavior is what is expected from this sort of configuration under the indicated loading.

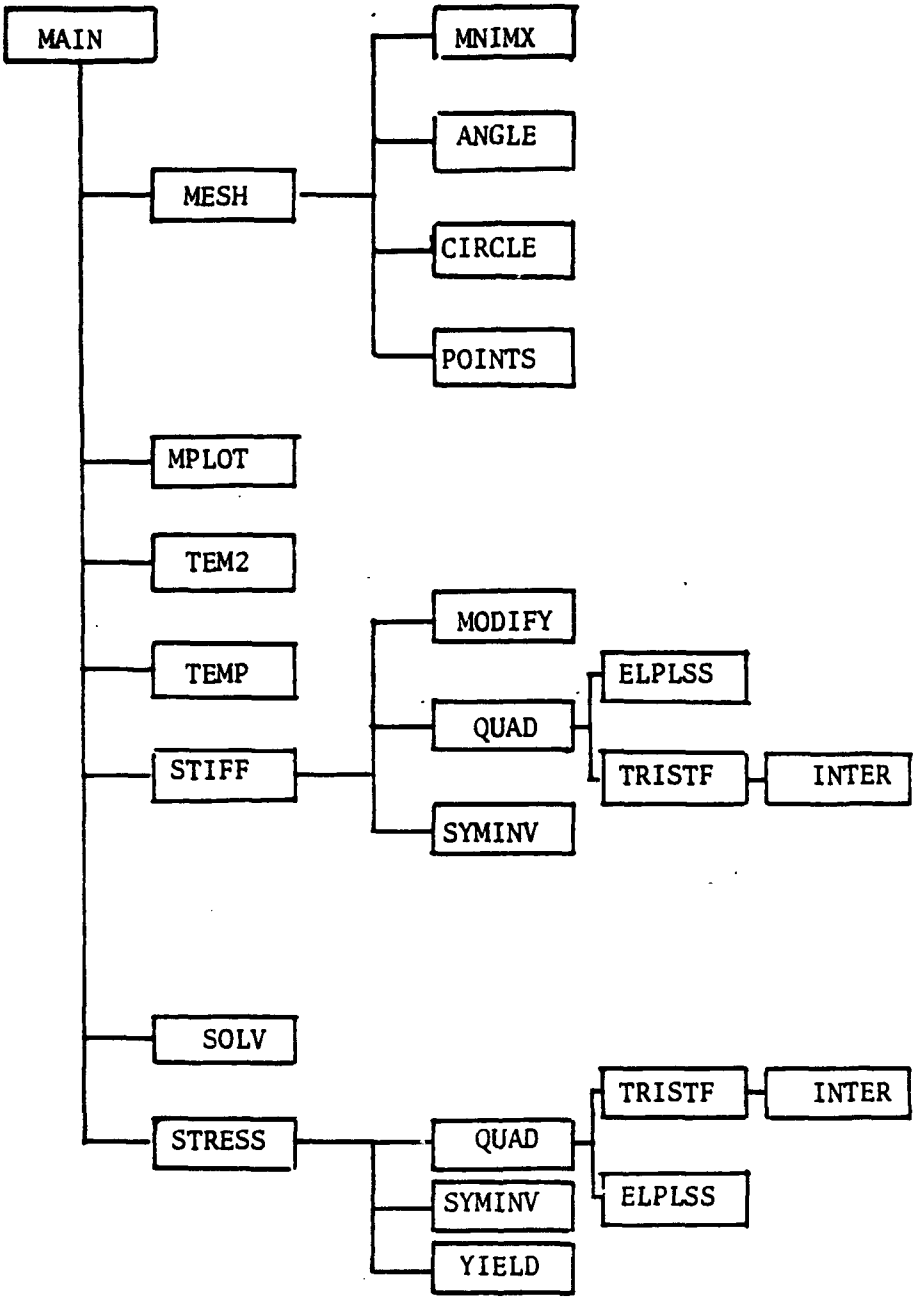

Figure 1. Flow Chart of SAGAEP.

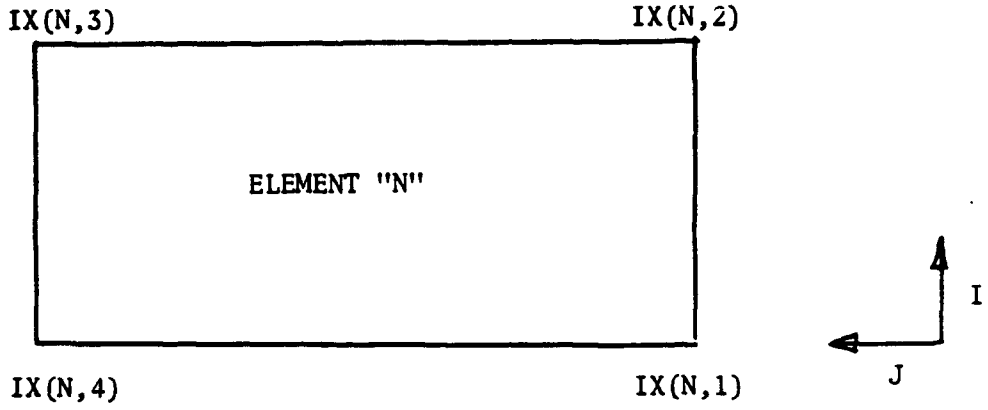

Figure 2. Nodal Numbering System for an Element Generated by SAGA.

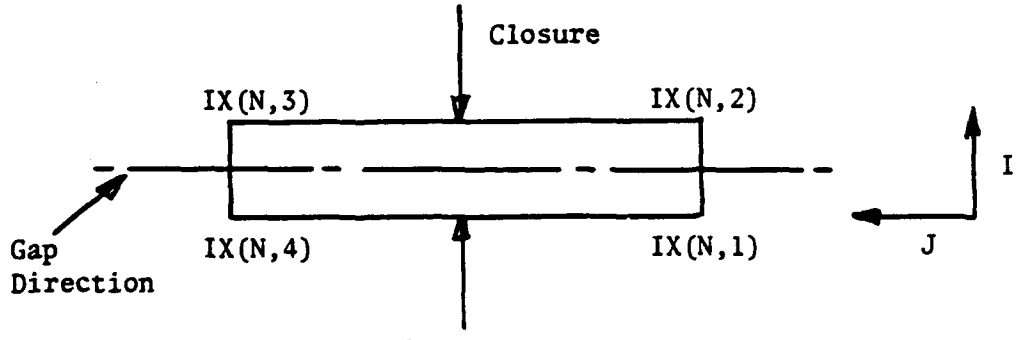

Figure 3. Gap Element Configuration for a Gap in J Direction.

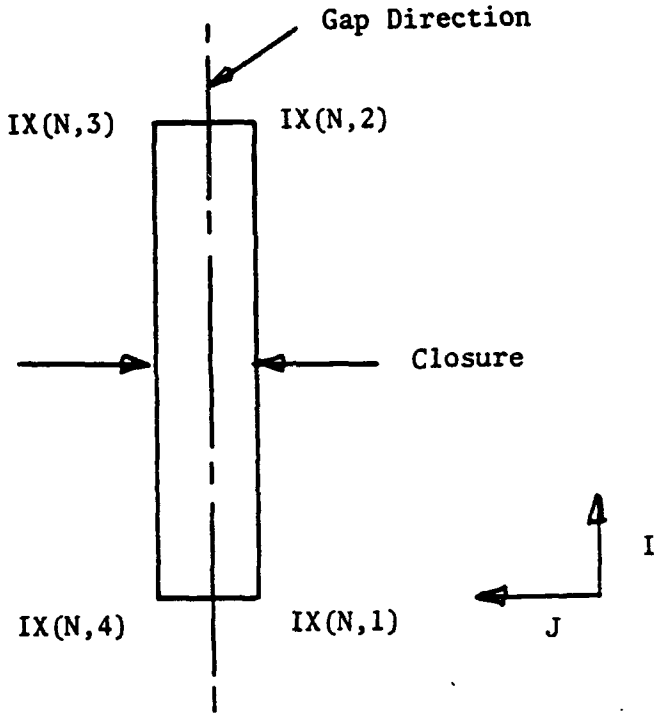

Figure 4. Gap Element Configuration for a Gap in I Direction.

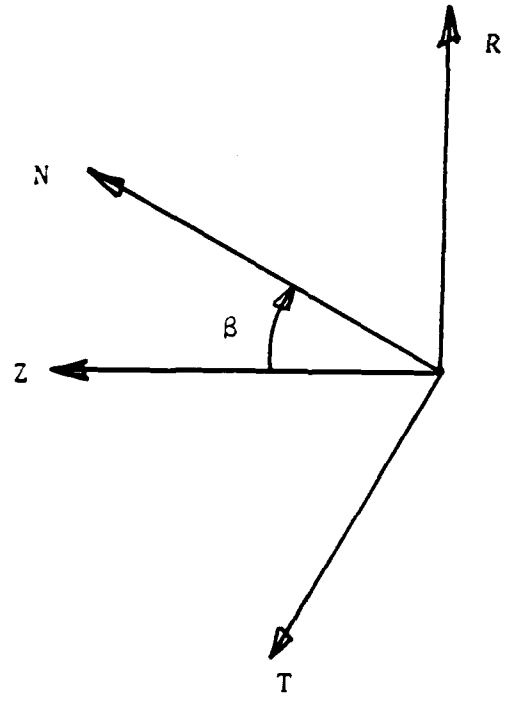

Figure 5. Definition of the Gap Element Orientation Angle.

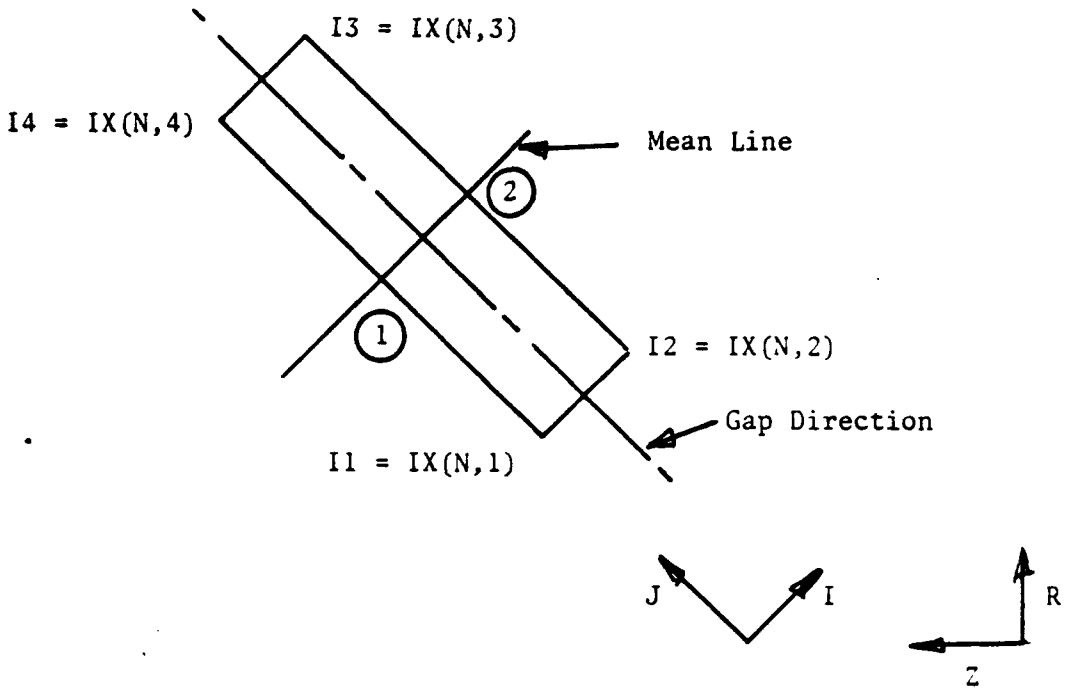

Figure 6. Gap Element Mean Line Used to Determine Orientation.

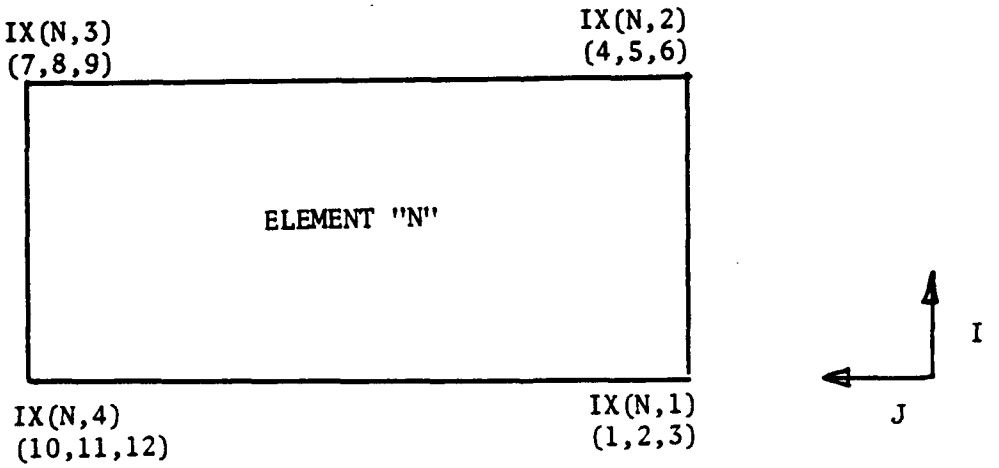

Figure 7. Degrees of Freedom for an Element in a Three-Dimensional Analysis. (Note: The Numbers in () Indicate Degrees of Freedom at Each Node.)

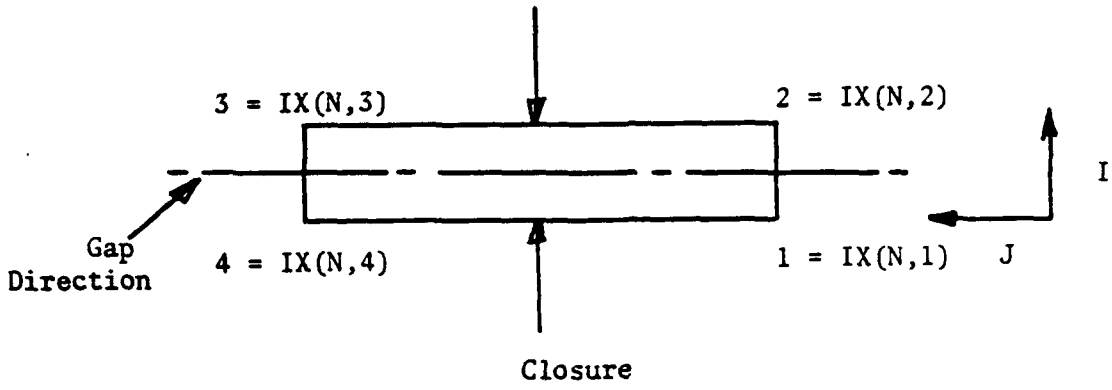

Figure 8. Gap in the J Direction Used to Illustrate Various Stiffness Modifications.

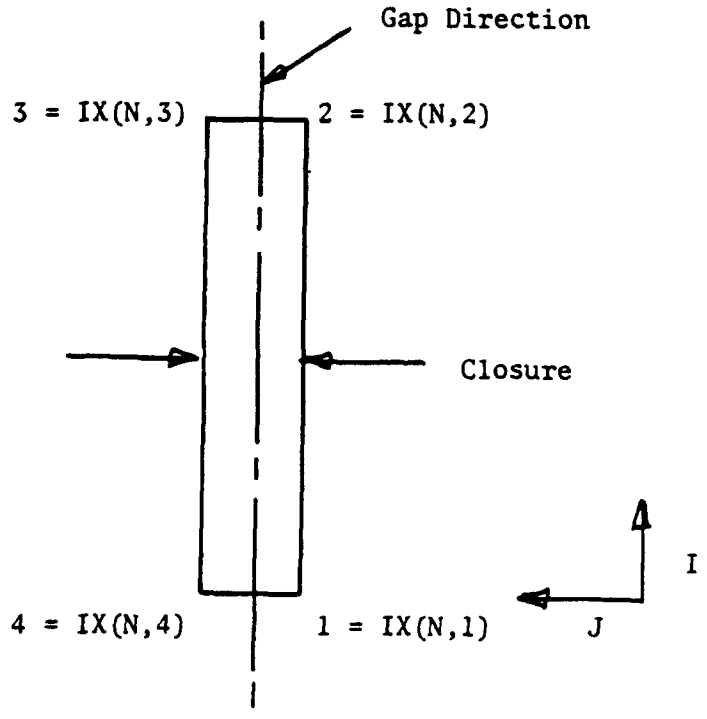

Figure 9. Gap in the I Direction Used to Illustrate Various Stiffness Modifications.

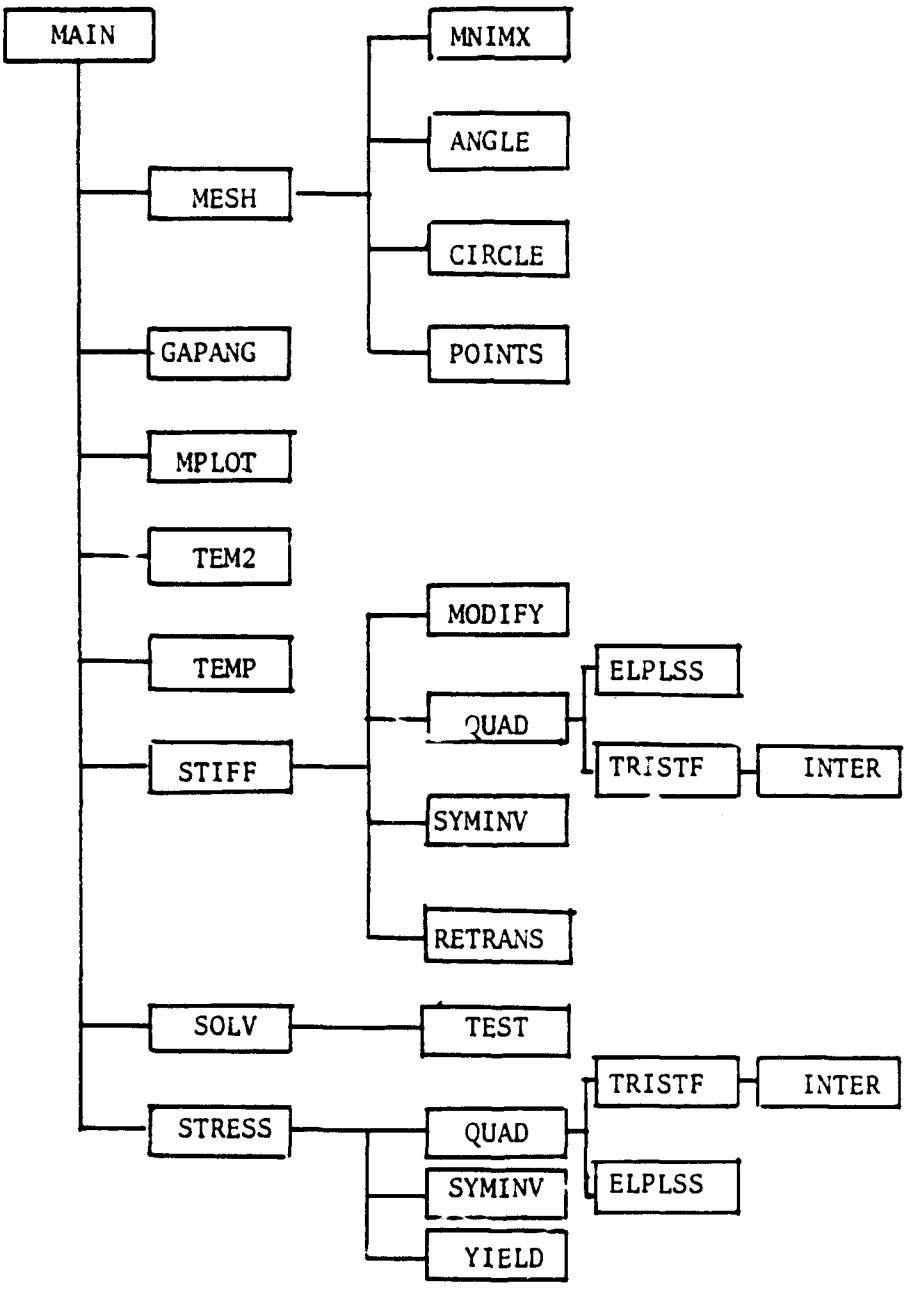

Figure 10. Flow Chart of SAAC Program.

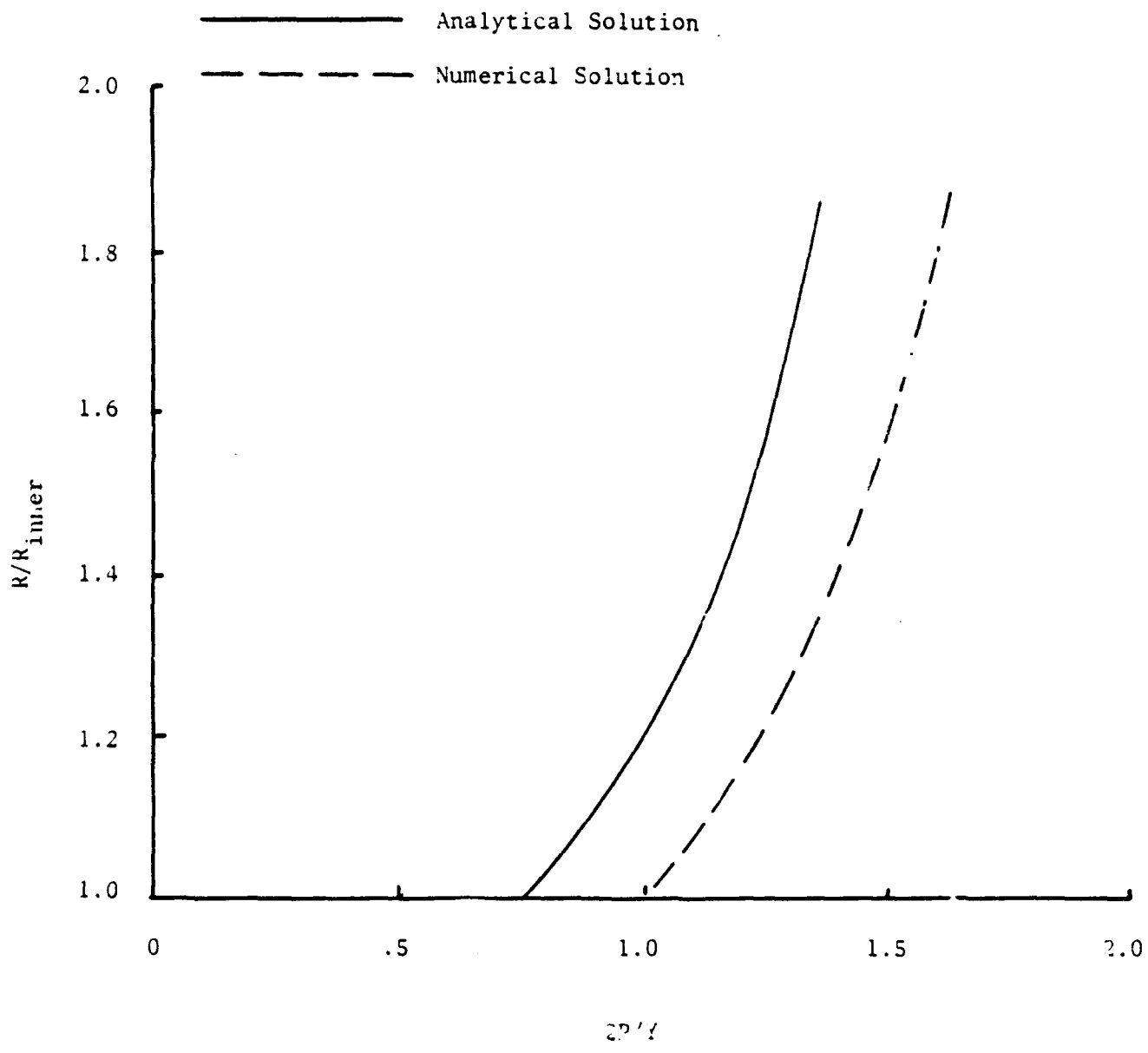

Figure 11. Elastic-Plastic Boundary as a Function of Pressure for the Perfectly Plastic Disc (Y = Yield Stress, R = Radius, P = Internal Pressure).

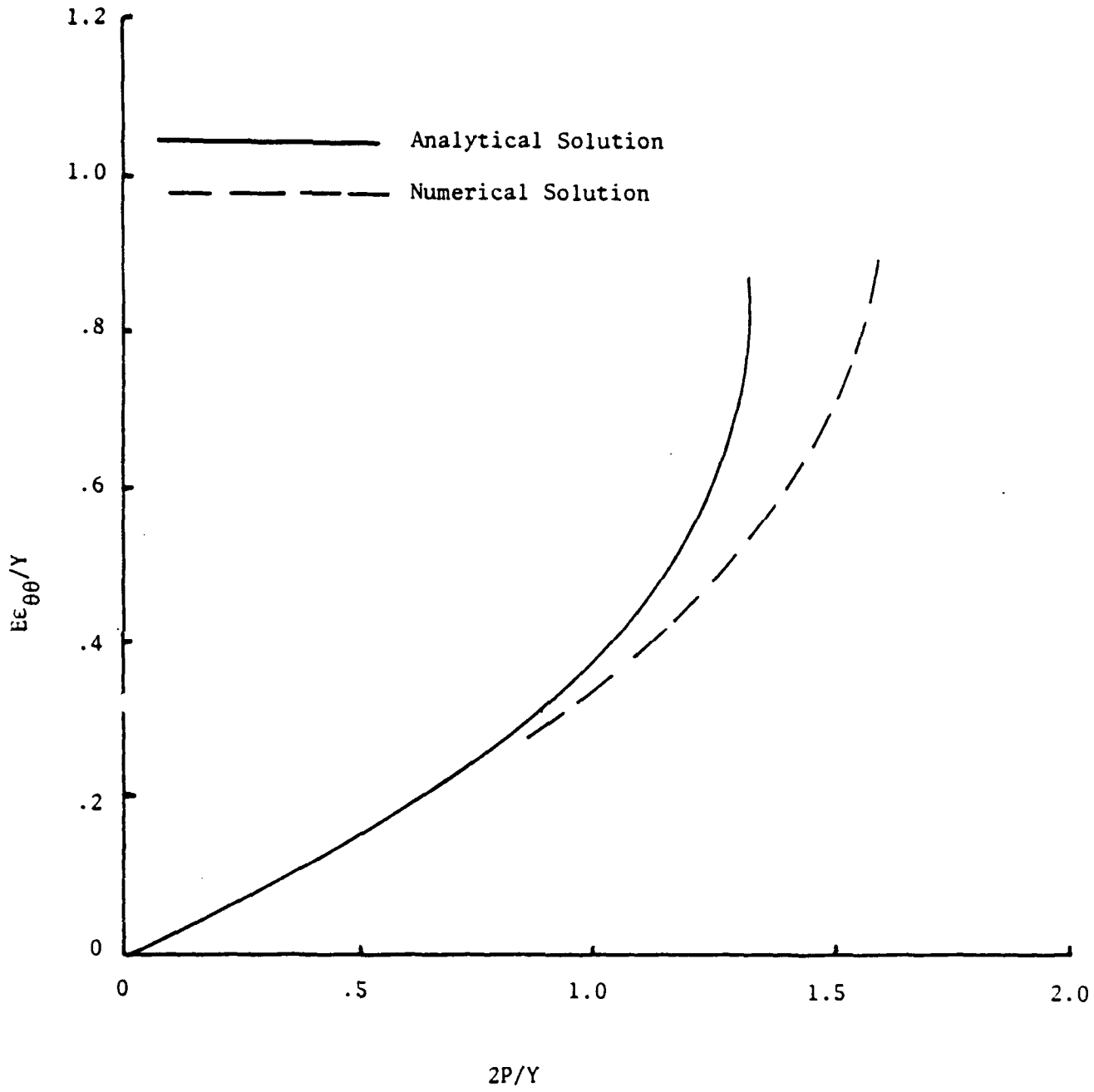

Figure 12. Outer Circumferential Strain as a Function of Pressure for the Perfectly Plastic Disc (E = Elastic Modulus).

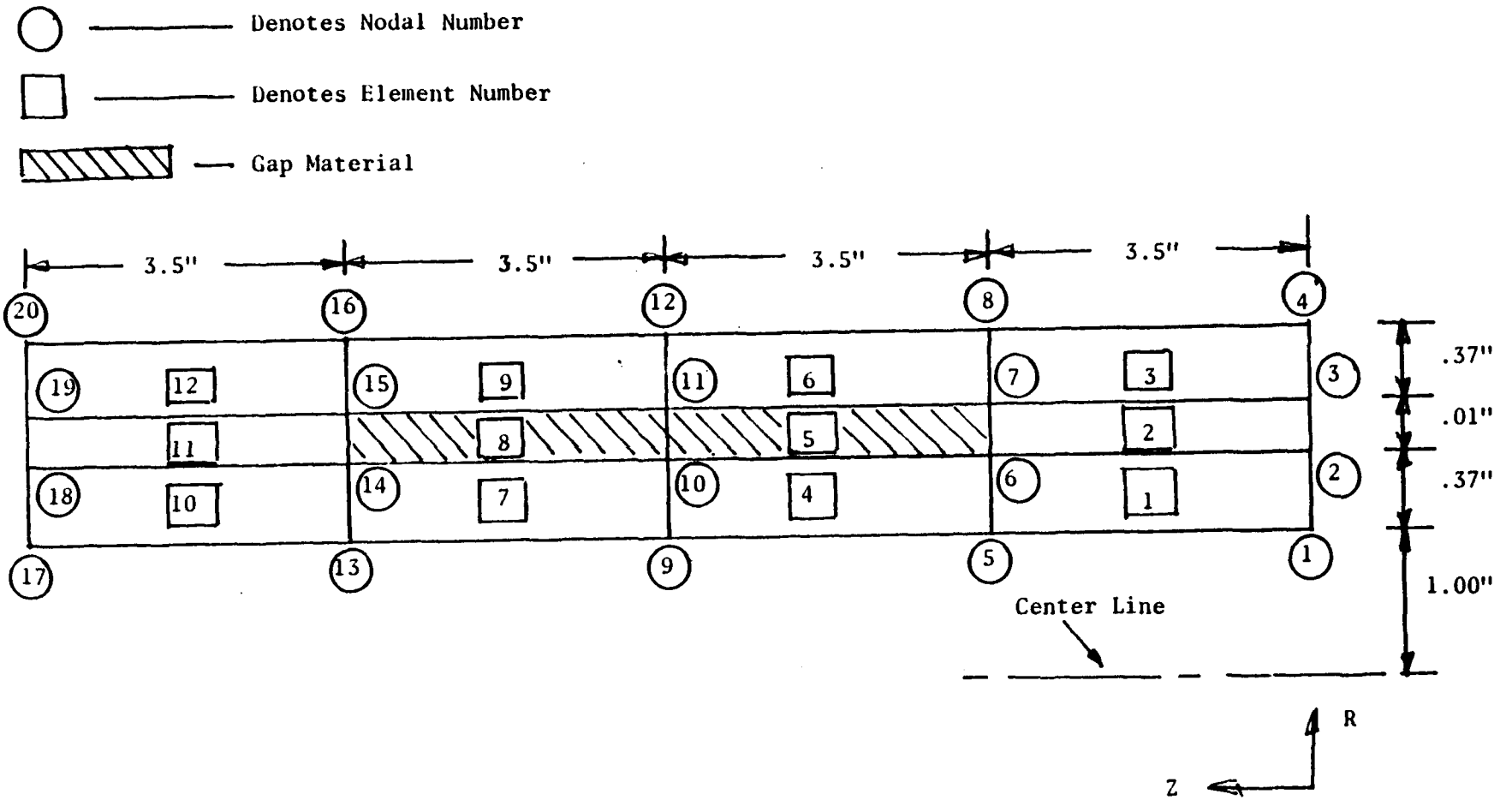

Figure 13. Numerical Example With Flat Gap and Coarse Grid.

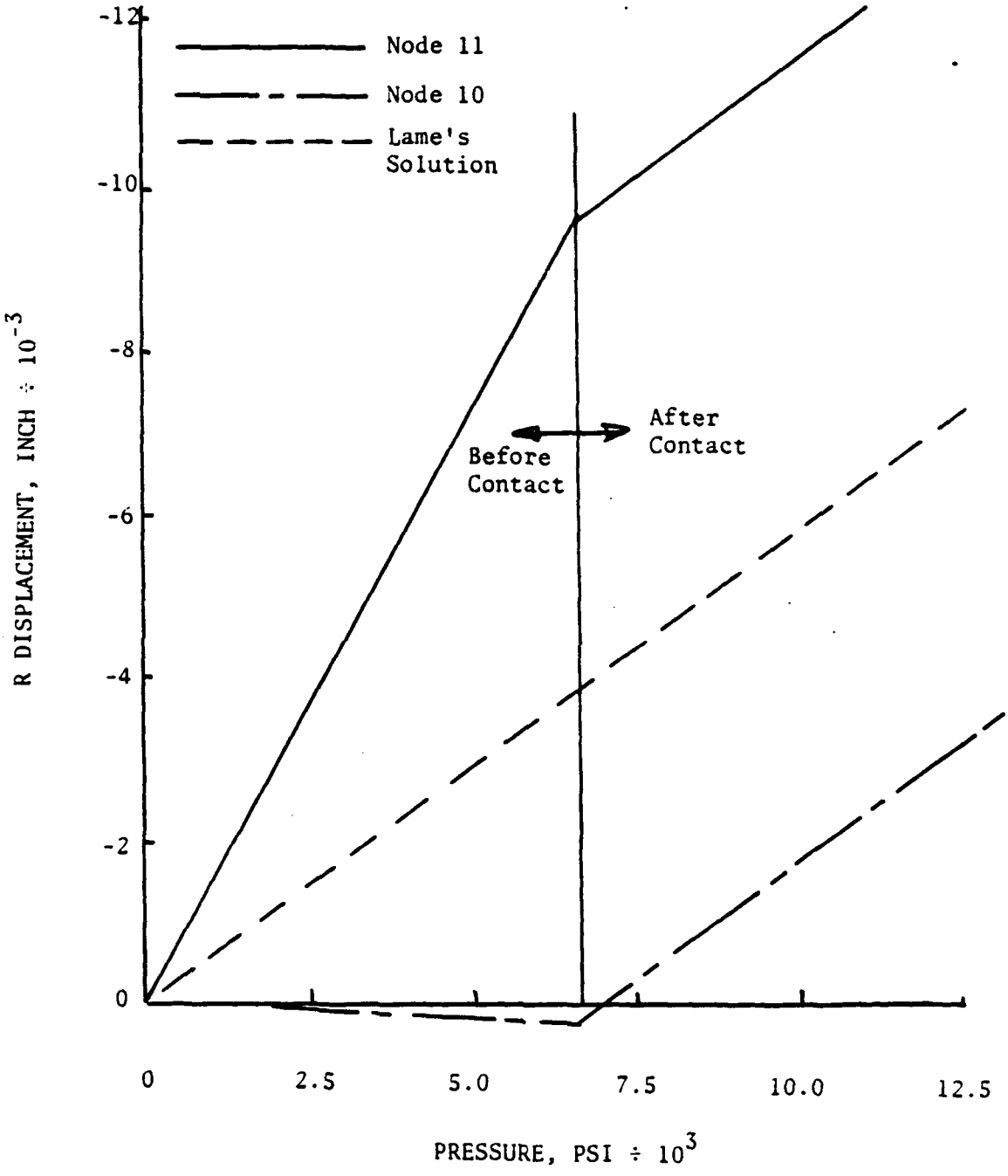

Figure 14. Radial Displacement as a Function of Pressure for the Flat Gap Example (Coarse Grid).

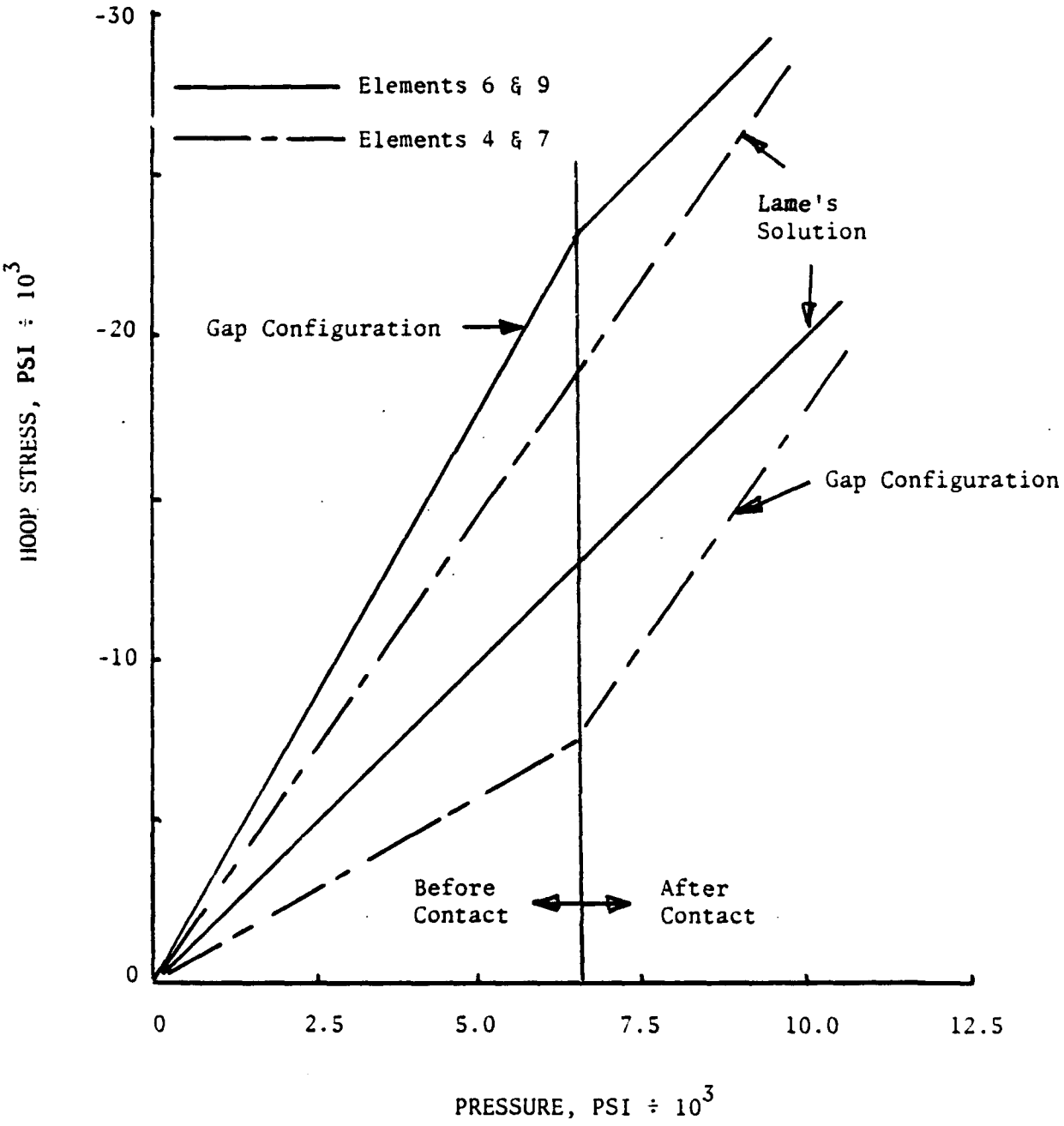

Figure 15. Hoop Stress as a Function of Pressure for the Flat Gap Example (Coarse Grid).

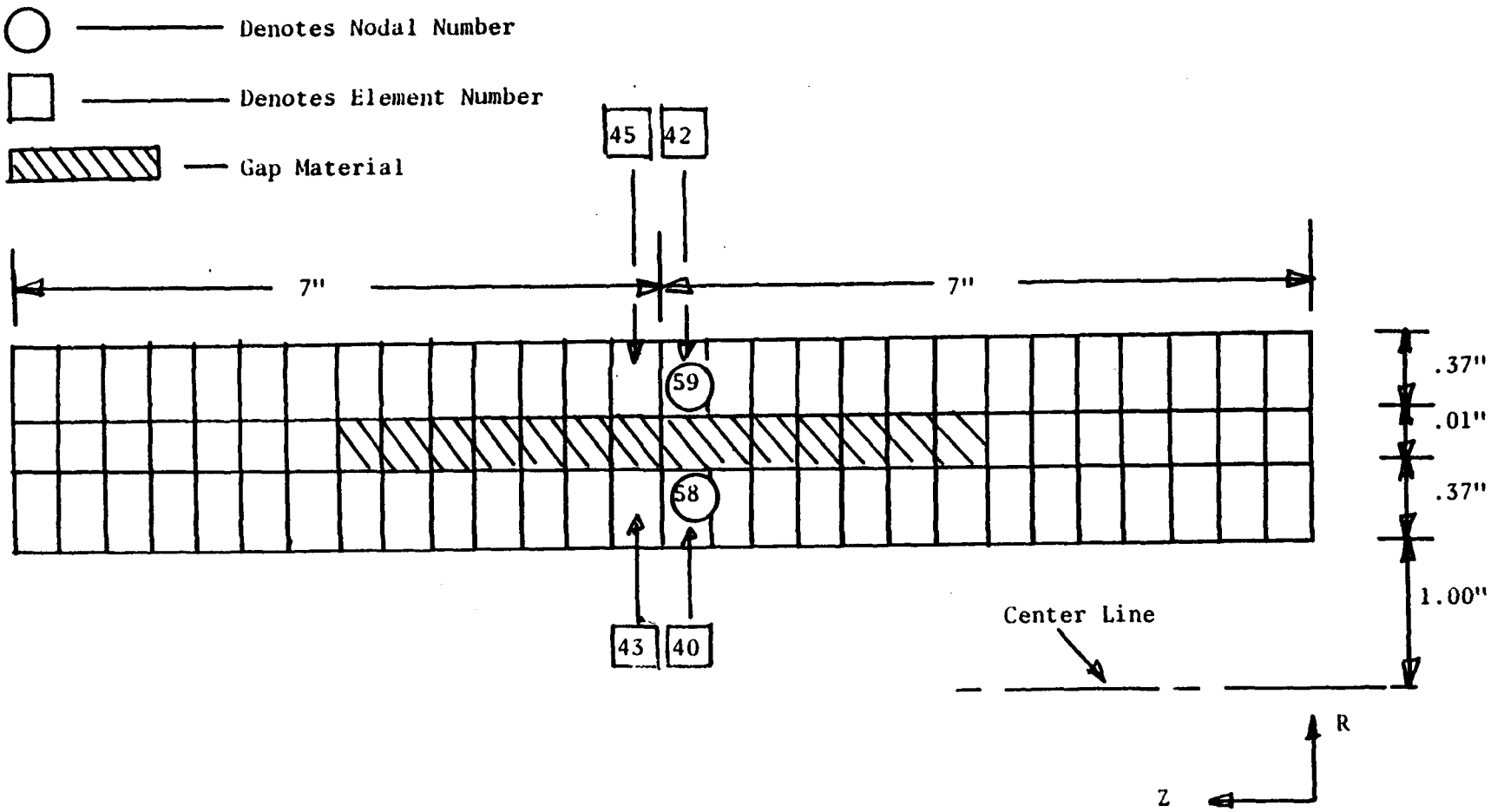

Figure 16. Numerical Example With Flat Gap and Fine Grid.

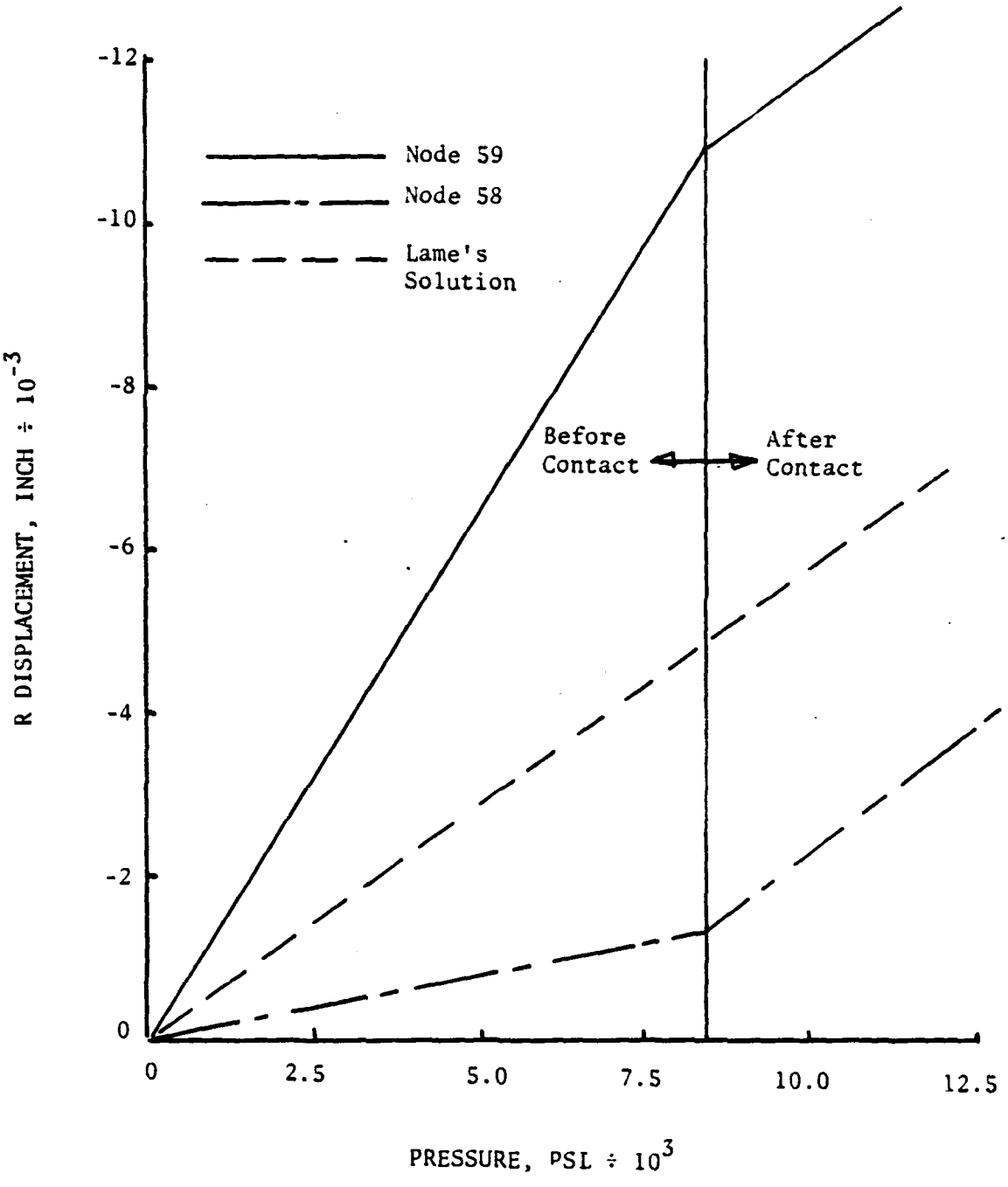

Figure 17. Radial Displacement as a Function of Pressure for the Flat Gap Example (Fine Grid).

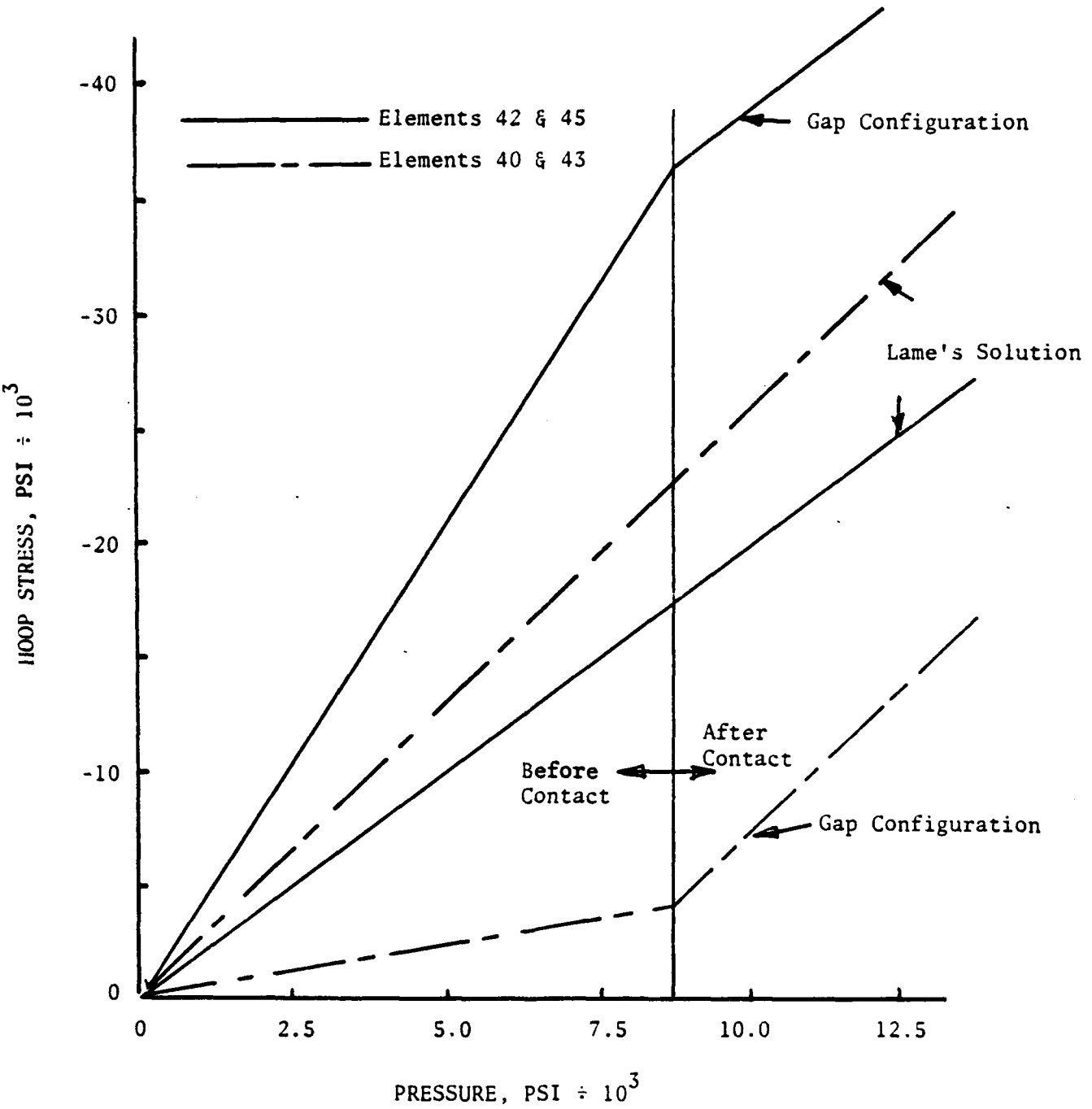

Figure 18. Hoop Stress as a Function of Pressure for the Flat Gap Example (Fine Grid).

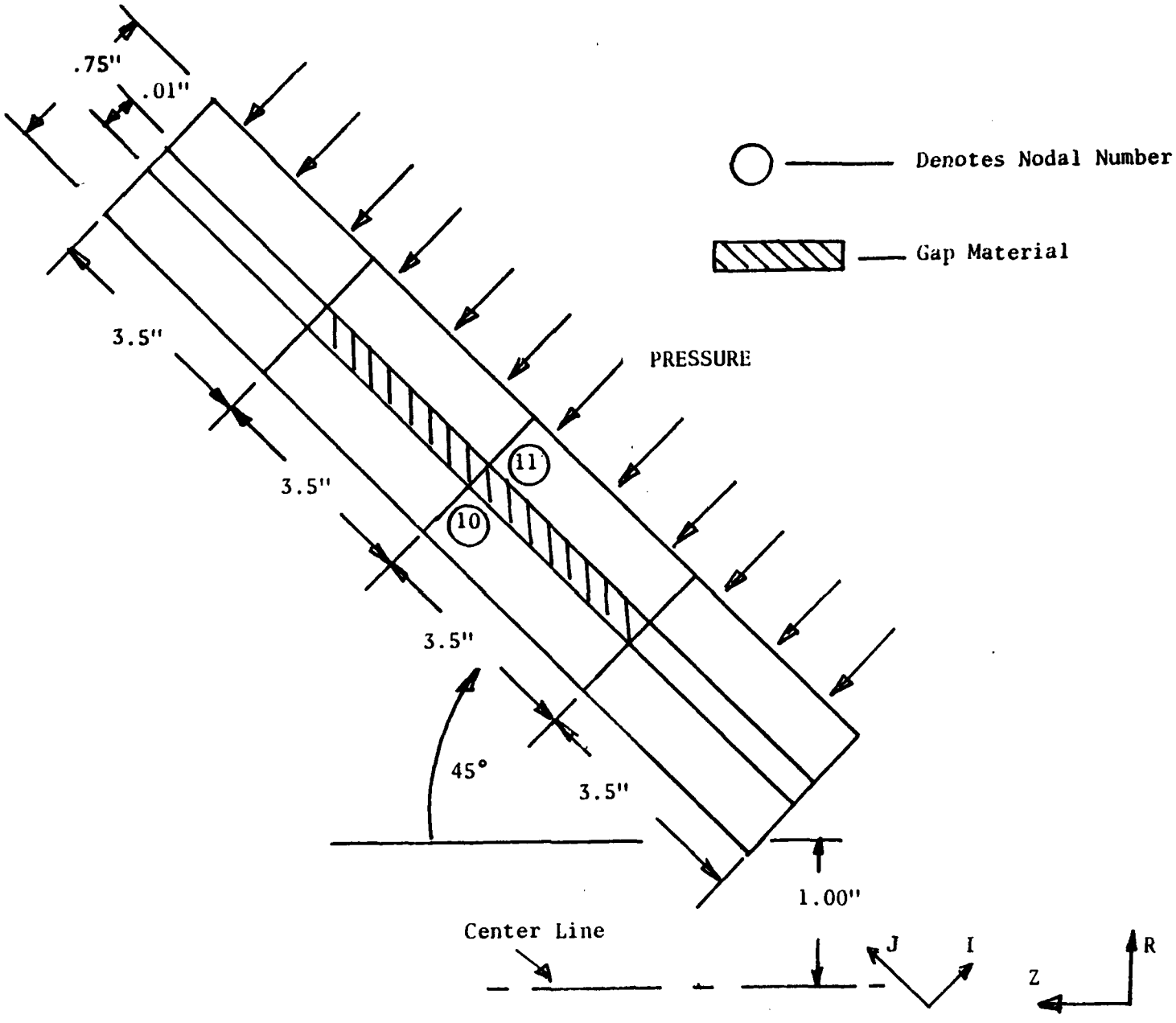

Figure 19. Numerical Example With Angled Gap.

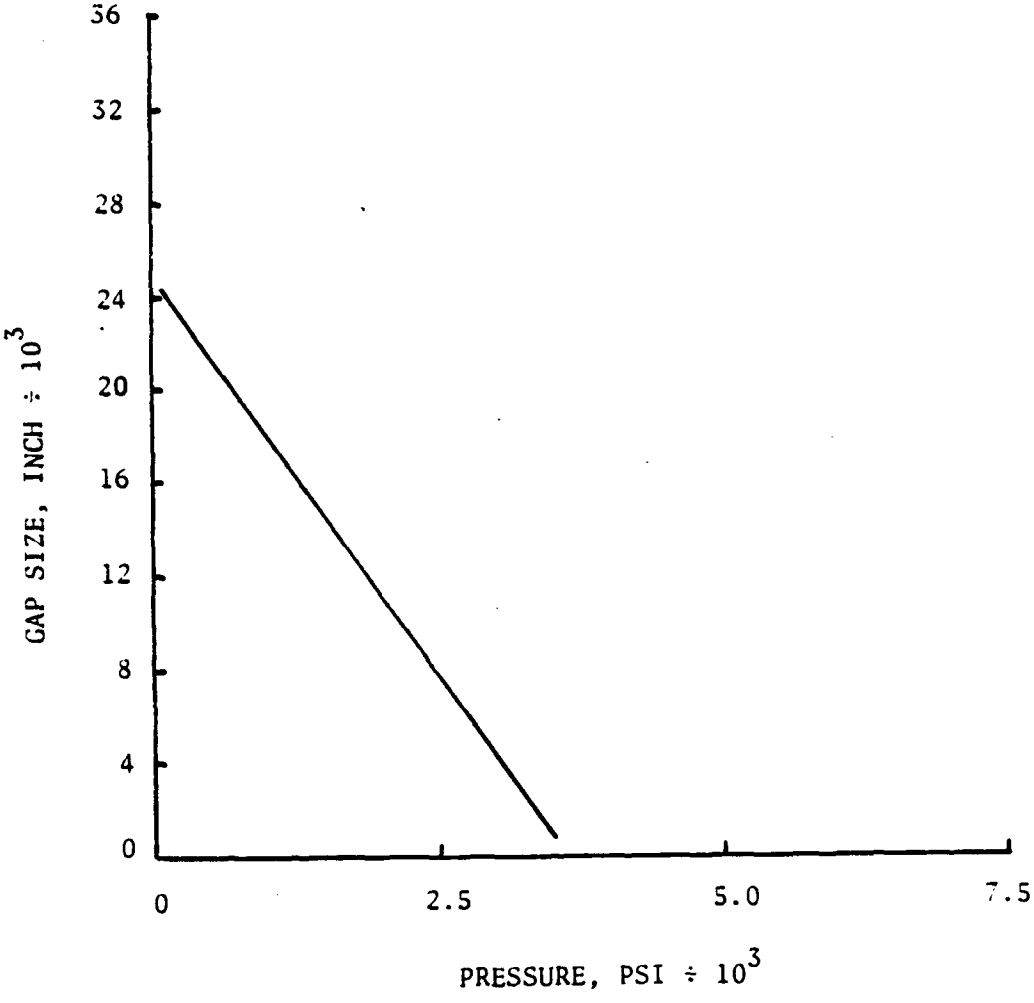

Figure 20. Gap Size as a Function of Pressure for the Angled Configuration.

INTENTIONALLY LEFT BLANK.

9. REFERENCES

Calladine, C. R. Engineering Plasticity. London: Pergamon Press, 1969.

Gaertner, R. "Investigation of Plane Elastic Contact Allowing for Friction." Computers and Structures, vol. 7, pp. 59–63, 1977.

Hill, R. "A Theory of Yielding and Plastic Flow of Anisotropic Metals." Proceedings of the Royal Aeronautical Society, vol. 193, 1948.

Hung, N. S., and G. de Saxce. "Frictionless Contact of Elastic Bodies by Finite Element Method and Mathematical Programming Technique." Computers and Structures, vol. 11, pp. 55–67, 1980.

Mahmoud, F. F., N. J. Salomon, and W. R. Marks. "A Direct Automated Procedure for Frictionless Contact Problems." International Journal for Numerical Methods in Engineering, vol. 18, pp. 245–257, 1982.

Shield R., and H. Ziegler. "On Prager's Hardening Rule." Journal of Applied Mathematics and Physics," vol. 9, 1958.

Stadter J. T., and R. O. Weiss. "Analysis of Contact Through Finite Element Gaps." Computers and Structures, vol. 10, pp. 867–873, 1979.

Zak, A. R. "Finite Element Computer Program for the Analysis of Layered Orthotropic Structures." BRL-CR-158, U.S. Army Ballistic Research Laboratory, Aberdeen Proving Ground, MD, 1974.

Zak, A. R. "Numerical Analysis of Laminated Orthotropic Composite Structures." BRL-CR-272, U.S. Army Ballistic Research Laboratory, Aberdeen Proving Ground, MD, November 1975.

Zak, A. R., J. N. Craddock, and W. H. Drysdale. "An Elastic-Plastic Analysis of Non-Axisymmetric Structures." Computers and Structures, vol. 10, pp. 841–846, 1979.

INTENTIONALLY LEFT BLANK.

APPENDIX:

INPUT CARDS FOR GAP COMPUTER PROGRAMS

INTENTIONALLY LEFT BLANK.

1. TITLE CARD

Format (20A4)

Columns	1–80	TITLE (Title for particular case)

2. CONTROL CARD

Format (6I5, F5.0, 6I5)

Columns	1–5	NNLA (Number of nonlinear approximations; NNLA = 1 for this version of the program.)
	6–10	NUMTC (Number of temperature cards; if -2, a constant temperature is specified.)
	11–15	NUMMAT (Number of different materials; 6 maximum)
	16–20	NUMPC (Number of boundary pressure cards; 200 maximum)
	21–25	NUMSC (Number of boundary shear cards; 200 maximum)
	26–30	NUMST (Number of boundary shear cards in tangential direction; 200 maximum)
	31–35	TREF (Reference temperature)
	36–40	INERT (This parameter decides if inertia loads will be present; INERT + 0 means zero values of axial acceleration and angular acceleration and velocity for each load increment.)
	41–45	NLINC (Number of load increments with time; NLINC ≥ 1)
	46–50	INCI (If INCI = 0, then inertia loads for each time increment will be equal to the inertia load for the first time increment.)
	51–55	INCF (If INCF = 0, then surface loads for each time increment will be the same as for first increment.)
	56–60	IPLOT (Plot parameter; 1 if plot required)
	61–65	LGAP (If LGAP = 1, then the gap direction will be parallel to the J-axis; if LGAP = 2, then the gap direction will be parallel to the I-axis.)

2a. TIME INCREMENT CARD

Note: This card is used only for elastic-viscoplastic option—omit for elastic-plastic version.

Format (E10.0)

Columns	1–10	DELTIM (Time increment)

3. MESH GENERATION CONTROL CARD

Format (5I5)

Columns	1–5	MAXI (Maximum value of I in mesh; 25 maximum)
	6–10	MAXJ (Maximum value of J in mesh; 100 maximum)
	11–15	NSEG (Number of line segment cards)
	16–20	NBC (Number of boundary condition cards)
	21–25	NMTL (Number of material block cards)

4. LINE SEGMENT CARDS

The order of line segment cards is immaterial, except when plots are requested; in this case, the line segment cards must define the perimeter of the solid continuously. The order of line segment cards defining internal straight lines is always irrelevant.

Format [3(2I3, 2F8.3), I5]

Columns	1–3	I coordinate of 1st point
	4–6	J coordinate of 1st point
	7–14	R coordinate of 1st point
	15–22	Z coordinate of 1st point
	23–25	I coordinate of 2nd point
	26–28	J coordinate of 2nd point
	29–36	R coordinate of 2nd point
	37–44	Z coordinate of 2nd point
	45–47	I coordinate of 3rd point

	48–50	J coordinate of 3rd point
	51–58	R coordinate of 3rd point
	59–66	Z coordinate of 3rd point
	67–71	Line segment type parameter

If the number in column 71 is

0	Point (input only 1st point)
1	Straight line (input only 1st and 2nd points)
2	Straight line as an internal diagonal (input only 1st and 2nd points)
3	Circular arc specified by 1st and 3rd points at the ends of the arc and 2nd point at the midpoint of the arc
4	Circular arc specified by 1st and 2nd points at the ends of the arc with the coordinates of the center of the arc given as the 3rd point (delete I and J for 3rd point)
5	Straight line as boundary diagonal for which I of 1st point is minimum for its row and/or I of 2nd point is minimum for its row (input only 1st and 2nd points)
6	Straight line as boundary diagonal for which I of 1st point and/or 2nd point is maximum for its row (input only 1st and 2nd points)

NOTE: In specifying a circular arc, the points are ordered such that a counterclockwise direction about the center is obtained upon moving along the boundary.

5. BOUNDARY CONDITION CARDS

Each card assigns a particular boundary condition to a block of elements bounded by I1, I2, J1, and J2. For a line, I1 = I2, or J1 = J2. For a point, I1 = I2, and J1 = J2.

Format (4I5, I10, 3F10.0)

Columns	1–5	Minimum I
	6–10	Maximum I
	11–15	Minimum J

16–20	Maximum J
21–30	Boundary condition code
31–40	Radial boundary condition code, XR
41–50	Axial boundary condition, XZ
51–60	Tangential boundary condition, XT

If the number in Columns 21–30 is

0	XR is the specified R-load, XZ is the specified Z-load, and XT is the specified θ-load.
1	XR is the specified R-displacement, XZ is the specified Z-load, and XT is the specified θ-load.
2	XR is the specified R-load, XZ is the specified Z-displacement, and XT is the specified θ-load.
3	XR is the specified R-displacement, XZ is the specified Z-displacement, and XT is the specified θ-load.
4	XR is the specified R-load, XZ is the specified Z-load, and XT is the specified θ-displacement.
5	XR is the specified R-displacement, XZ is the specified Z-load, and XT is the specified θ-displacement.
6	XR is the specified R-load, XZ is the specified Z-displacement, and XT is the specified θ-displacement.
7	XR is the specified R-displacement, XZ is the specified Z-displacement, and XT is the specified θ-displacement.

6. MATERIAL BLOCK ASSIGNMENT CARD

Each card assigns a material definition number to a block of elements defined by the I, J coordinates.

Format (5I5, 2F10.0, 2I5)

Columns	1–5	Material definition number (1 through 6)
	6–10	Minimum I
	11–15	Maximum I
	16–20	Minimum J
	21–25	Maximum J
	26–35	Material principal property inclination angle BETA which defines N-S plane orientation relative to z direction (see Figure 4)
	36–45	Material principal property inclination angle ALPHA which defines the orientation of the N-T plane relative to the r-z plane (see Figure 4)
	46–50	IANG (If IANG = 0, then ALPHA is same for total material block. If IANG = 1, the ALPHA varies in sign in the I direction from element to element every NANG elements. This will allow for equal but opposite helical angles.)
	51–55	NANG (Number of elements in the I direction with the same ALPHA)

NOTE: Gap elements will be identified by a material definition number of 2.

7. PLOT TITLE CARD

Format (20A4)

Columns	1–80	Title (Title printed under each plot)

8. PLOT GENERATION INFORMATION CARD

Format (2F10.0)

Columns	1–10	RMAX (Maximum r coordinate of mesh)
	11–20	ZMAX (Maximum z coordinate of mesh)

NOTE: Use only if IPLOT = 1 (plot required).

9. TEMPERATURE FIELD INFORMATION CARDS

If NUMTC in columns 6–10 of the CONTROL CARD is greater than 1, the temperature field is given on cards. One card must be supplied for each point for which a temperature is specified.

Format (3F10.0)

Columns	1–10	R coordinate
	11–20	Z coordinate
	21–30	Temperature

If NUMTC in columns 6–10 of the CONTROL CARD is -2, a constant temperature field is specified; the value is given on a single card.

Format (F10.0)

Columns	1–10	Temperature

10. MATERIAL PROPERTY INFORMATION CARDS

Cards 10 to 11 (11a for elastic-viscoplastic option) must be specified for each material (maximum of 6).

a. MATERIAL IDENTIFICATION CARD

Format (2I5, 2F10.0)

Columns	1–5	Material identification number
	6–10	Number of temperatures for which properties are given (12 maximum)
	11–20	Mass density of material (if required)
	21–30	Thermal expansion parameter (if 1, free thermal expansion on the material property cards; otherwise, coefficients of thermal expansion are on the material property cards.)

b. MATERIAL PROPERTY CARDS

Two cards are required for each temperature.

First Card

Format (7F10.0)

Columns	1–10	Temperature
	11–20	Modulus of elasticity, E_N
	21–30	Modulus of elasticity, E_S

	31–40	Modulus of elasticity, E_T
	41–50	Poisson's ratio, ν_{NS}
	51–60	Poisson's ratio, ν_{NT}
	61–70	Poisson's ratio, ν_{ST}

Second Card

Format (6F10.0)

Columns	1–10	Shear Modulus, G_{NS}
	11–20	Shear Modulus, G_{ST}
	21–30	Shear Modulus, G_{TN}
	31–40	$\alpha_N T$ or α_N
	41–50	$\alpha_S T$ or α_S
	51–60	$\alpha_T T$ or α_T

11. YIELD STRESS CARDS

(not needed in elastic version)

Format (7F10.0)

Columns	1–10	Yield stress in tension in N direction
	11–20	Yield stress in tension in S direction
	21–30	Yield stress in tension in T direction
	31–40	Yield stress in shear in NS direction
	41–50	Yield stress in shear in NT direction
	51–60	Yield stress in shear in TS direction
	61–70	Hardening parameter; C

11a. VISCOSITY CARD

NOTE: This card used only for elastic-viscoplastic option; omit for elastic-plastic version.

Format (E10.0)

Columns	1–10	ETA (viscosity coefficient)

12. INERTIA LOAD CARD

Format (3F10.0)

Starting with this input card and including the boundary force cards, this data is to be input as a block for each load step, that is, NLINC times. There are the following exceptions to this:

(a) If INERT = 0, then this card is to be omitted completely (no inertia load).

(b) If INCI = 0, then this card is not repeated, but appears in first block only (the inertia loads are constant for each load step).

(c) If INCF = 0, then the following boundary pressure and shear cards are to be given only for the first block and not repeated again (the pressure and shear loads are constant for each load increment).

Columns	1–10	ACELZ (axial acceleration)
	11–20	ANGVEL (angular velocity)
	21–30	ANGACC (angular acceleration)

13. BOUNDARY PRESSURE CARDS

One card is required for each boundary element which is subjected to a normal pressure; that is, the number of these cards is NUMPC for each load increment.

Format (2I5, F10.0)

Columns	1–5	Nodal point M
	6–10	Nodal point N
	11–20	Normal pressure

As shown in Figure A-1, the boundary element must be on the left when progressing from M to N. Surface normal tension is input as a negative pressure.

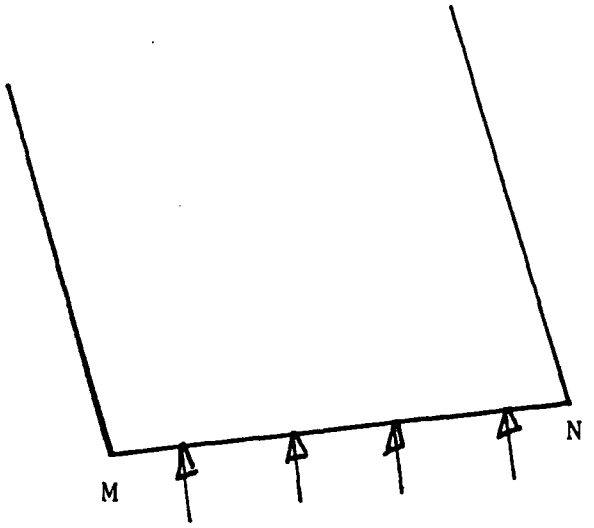

Figure A-1. Example of Boundary Pressure Loading.

14. BOUNDARY SHEAR CARDS

One card is required for each boundary element which is subjected to surface shear; that is, the number of these cards is NUMSC for each load increment.

Format (2I5, F10.0)

Columns		
	1–5	Nodal point M
	6–10	Nodal point N
	11–20	Surface shear

As shown in Figure A-2, the boundary element must be on the left when progressing from M to N. The positive sense of the shear is from M to N.

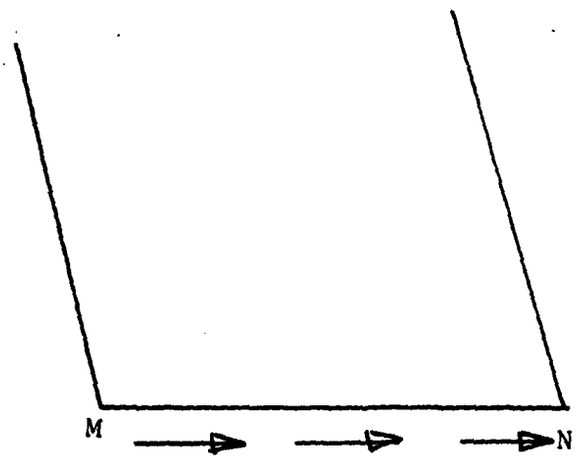

Figure A-2. Example of Boundary Shear Loading.

15. BOUNDARY TRANSVERSE SHEAR CARDS

One card is required for each boundary element which is subject to transverse shear; that is, the number of these cards is NUMSC for each load increment.

Format (2I5, F10.0)

Columns	1–5	Nodal point M
	6–10	Nodal point N
	11–20	Surface transverse shear

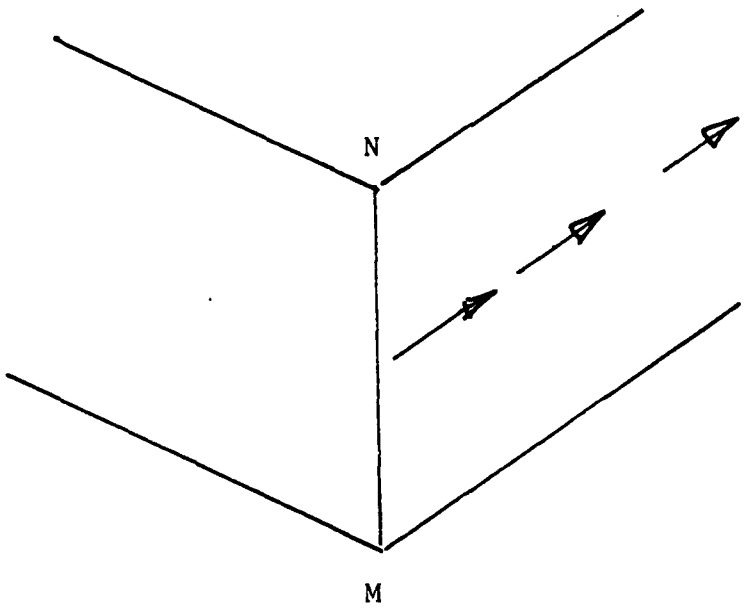

Figure A-3. Example of Boundary Transverse Shear Loading.

INTENTIONALLY LEFT BLANK.

USER EVALUATION SHEET/CHANGE OF ADDRESS

This laboratory undertakes a continuing effort to improve the quality of the reports it publishes. Your comments/answers below will aid us in our efforts.

1. Does this report satisfy a need? (Comment on purpose, related project, or other area of interest for which the report will be used.) _____

2. How, specifically, is the report being used? (Information source, design data, procedure, source of ideas, etc.) _____

3. Has the information in this report led to any quantitative savings as far as man-hours or dollars saved, operating costs avoided, or efficiencies achieved, etc? If so, please elaborate. _____

4. General Comments. What do you think should be changed to improve future reports? (Indicate changes to organization, technical content, format, etc.) _____

BRL Report Number BRL-CR-674 Division Symbol _____

Check here if desire to be removed from distribution list. ____

Check here for address change. ____

Current address: Organization _____
Address _____

DEPARTMENT OF THE ARMY
Director
U.S. Army Ballistic Research Laboratory
ATTN: SLCBR-DD-T
Aberdeen Proving Ground, MD 21005-5066

OFFICIAL BUSINESS

BUSINESS REPLY MAIL
FIRST CLASS PERMIT No 0001, APG, MD

Postage will be paid by addressee.

NO POSTAGE NECESSARY IF MAILED IN THE UNITED STATES

Director
U.S. Army Ballistic Research Laboratory
ATTN: SLCBR-DD-T
Aberdeen Proving Ground, MD 21005-5066

No. of Copies	Organization
2	Administrator Defense Technical Info Center ATTN: DTIC-DDA Cameron Station Alexandria, VA 22304-6145
1	Commander U.S. Army Materiel Command ATTN: AMCDRA-ST 5001 Eisenhower Avenue Alexandria, VA 22333-0001
1	Commander U.S. Army Laboratory Command ATTN: AMSLC-DL 2800 Powder Mill Road Adelphi, MD 20783-1145
2	Commander U.S. Army Armament Research, Development, and Engineering Center ATTN: SMCAR-IMI-I Picatinny Arsenal, NJ 07806-5000
2	Commander U.S. Army Armament Research, Development, and Engineering Center ATTN: SMCAR-TDC Picatinny Arsenal, NJ 07806-5000
1	Director Benet Weapons Laboratory U.S. Army Armament Research, Development, and Engineering Center ATTN: SMCAR-CCB-TL Watervliet, NY 12189-4050
(Unclass. only)1	Commander U.S. Army Armament, Munitions and Chemical Command ATTN: AMSMC-IMF-L Rock Island, IL 61299-5000
1	Director U.S. Army Aviation Research and Technology Activity ATTN: SAVRT-R (Library) M/S 219-3 Ames Research Center Moffett Field, CA 94035-1000

No. of Copies	Organization
1	Commander U.S. Army Missile Command ATTN: AMSMI-RD-CS-R (DOC) Redstone Arsenal, AL 35898-5010
1	Commander U.S. Army Tank-Automotive Command ATTN: ASQNC-TAC-DIT (Technical Information Center) Warren, MI 48397-5000
1	Director U.S. Army TRADOC Analysis Command ATTN: ATRC-WSR White Sands Missile Range, NM 88002-5502
1	Commandant U.S. Army Field Artillery School ATTN: ATSF-CSI Ft. Sill, OK 73503-5000
(Class. only)1	Commandant U.S. Army Infantry School ATTN: ATSH-CD (Security Mgr.) Fort Benning, GA 31905-5660
(Unclass. only)1	Commandant U.S. Army Infantry School ATTN: ATSH-CD-CSO-OR Fort Benning, GA 31905-5660
1	Air Force Armament Laboratory ATTN: WL/MNOI Eglin AFB, FL 32542-5000

Aberdeen Proving Ground

2	Dir, USAMSAA ATTN: AMXSY-D AMXSY-MP, H. Cohen
1	Cdr, USATECOM ATTN: AMSTE-TC
3	Cdr, CRDEC, AMCCOM ATTN: SMCCR-RSP-A SMCCR-MU SMCCR-MSI
1	Dir, VLAMO ATTN: AMSLC-VL-D
10	Dir, BRL ATTN: SLCBR-DD-T

No. of
Copies Organization

2 Director
Benet Weapons Laboratory
U.S. Army Armament Research,
Development, and Engineering Center
ATTN: SMCAR-CCB,
J. Vasilakis
J. Zweig
Watervliet, NY 12189-5000

4 Commander
U.S. Army Armament Research,
Development, and Engineering Center
ATTN: SMCAR-CCH-T, S. Musalli
SMCAR-CC,
J. Hedderich
E. Fennell
R. Price
Picatinny Arsenal, NJ 07806-5000

1 Commander
U.S. Army Armament Research,
Development, and Engineering Center
ATTN: SMCAR-TD, T. Davidson
Picatinny Arsenal, NJ 07806-5000

2 Director
US Army Materials Technology Laboratory
ATTN: SLCMT-MEC,
B. Halpin
T. Chou
Watertown, MA 02172-0001

2 Director
Lawrence Livermore National Laboratory
ATTN: S. DeTeresa
R. M. Christensen
P.O. Box 808
Livermore, CA 94550

4 Director
Sandia National Laboratories
Applied Mechanics Department,
Division-8241
ATTN: C. W. Robinson
G. A. Benedetti
K. Perano
W. Kawahara
P.O. Box 969
Livermore, CA 94550-0096

No. of
Copies Organization

2 Battelle Pacific Northwest Laboratory
ATTN: M. Smith
M. Garnich
P.O. Box 999
Richland, WA 99352

1 Director
Los Alamos National Laboratory
ATTN: D. Rabern
WX-4 Division, Mail Stop G-787
P.O. Box 1663
Los Alamos, NM 87545

2 David Taylor Research Center
ATTN: R. Rockwell
W. Phyillaier
Bethesda, MD 20054-5000

1 Zak Technologies, Inc.
ATTN: Dr. Adam R. Zak
2310 Belmore Dr.
Champaign, IL 61821